

8. SITE 780¹

Shipboard Scientific Party²

HOLE 780A

Date occupied: 4 March 1989
Date departed: 5 March 1989
Time on hole: 21 hr, 15 min
Position: 19°32.51'N, 146°39.27'E
Bottom felt (rig floor; m, drill-pipe measurement): 3097.0
Distance between rig floor and sea level (m): 11.1
Water depth (drill-pipe measurement from sea level, m): 3086.8
Total depth (rig floor, m): 3101.4
Penetration (m): 3.5
Number of cores: 1
Total length of cored section (m): 3.5
Total core recovered (m): 3.54
Core recovery (%): 101
Oldest sediment cored:
Depth (mbsf): 3.54
Nature: silt-sized serpentine
Earliest age: late Pleistocene

HOLE 780B

Date occupied: 6 March 1989
Date departed: 6 March 1989
Time on hole: 23 hr
Position: 19°32.47'N, 146°39.22'E
Bottom felt (rig floor; m, drill-pipe measurement): 3105.1
Distance between rig floor and sea level (m): 11.1
Water depth (drill-pipe measurement from sea level, m): 3094.0
Total depth (rig floor, m): 3123.3
Penetration (m): 18.2
Number of cores: 2
Total length of cored section (m): 18.2
Total core recovered (m): 10.34
Core recovery (%): 56.6
Oldest sediment cored:
Depth (mbsf): 10.29
Nature: silt-sized serpentine
Earliest age: late Pleistocene

HOLE 780C

Date occupied: 6 March 1989
Date departed: 9 March 1989

Time on hole: 2 days, 23 hr, 30 min
Position: 19°32.53'N, 146°39.21'E
Bottom felt (rig floor; m, drill-pipe measurement): 3094.5
Distance between rig floor and sea level (m): 11.1
Water depth (drill-pipe measurement from sea level, m): 3083.4
Total depth (rig floor, m): 3258.0
Penetration (m): 163.5
Number of cores: 18
Total length of cored section (m): 163.5
Total core recovered (m): 14.4
Core recovery (%): 8.8
Oldest sediment cored:
Depth (mbsf): 33.7
Nature: silt-sized serpentine
Earliest age: middle Pleistocene(?)
Measured velocity (km/s): 1.5–2
Hard rock:
Depth (mbsf): 33.7
Nature: serpentized ultramafic rocks
Measured velocity (km/s): 5–6

HOLE 780D

Date occupied: 9 March 1989
Date departed: 10 March 1989
Time on hole: 1 day, 19 hr, 15 min
Position: 19°32.55'N, 146°39.20'E
Bottom felt (rig floor; m, drill-pipe measurement): 3100.1
Distance between rig floor and sea level (m): 11.2
Water depth (drill-pipe measurement from sea level, m): 3088.9
Total depth (rig floor, m): 3132.5
Penetration (m): 32.4
Number of cores: 7
Total length of cored section (m): 32.4
Total core recovered (m): 9.09
Core recovery (%): 28
Oldest sediment cored:
Depth (mbsf): 32.4
Nature: sandy silt-sized serpentine
Earliest age: Pleistocene (?)

Principal results: Site 780 is situated on the west-southwest side of the summit of Conical Seamount, about 2 nmi from the flank Sites 778 and 779. Site selection was based on *Alvin* submersible dives that indicated this area was covered with sediment and marked by active venting of fluids and precipitation of material from solution. The principal objectives of this site were to investigate (1) the physical properties and mineralogy of the serpentine flow materials and entrained clasts from the center of the diapir, (2) the composition and source of fluids associated with these materials, and (3) the potential for ore deposition within the seamount. In addition, this site was expected to provide further information

¹ Fryer, P., Pearce, J. A., Stokking, L. B., et al., 1990. *Proc. ODP, Init. Repts.*, 125: College Station, TX (Ocean Drilling Program).

² Shipboard Scientific Party is as given in list of participants preceding the contents.

about some of the objectives of the flank sites; in particular the nature, composition, and metamorphism of the forearc lithosphere and the construction of the seamount.

A total of four holes were drilled: Hole 780A was cored with an APC and recovered only 3.5 m of sediment; Hole 780B was drilled with an RCB to a depth of 18.2 mbsf with 57% recovery; Hole 780C was drilled with an RCB to a depth of 163.5 mbsf with 9% recovery; and Hole 780D was drilled with an XCB to a depth of 32.4 mbsf with 28% recovery. Overall, success in drilling at this site was constrained by the interbedding of hard serpentinitized peridotite and very soft, apparently fluid-charged, unconsolidated serpentine.

Two major lithologic units were recovered at Site 780: Unit I (0–3.5 mbsf in Hole 780A; 0–18.2 mbsf in Hole 780B; 0–14.0 mbsf in Hole 780C; and 0–15.4 mbsf in Hole 780D) comprises middle Pleistocene(?) to Holocene(?), sand- and silt-sized serpentine having rare intervals of foraminifer-rich serpentine clay and serpentine-rich silty-clay; and Unit II (14.0–163.5 mbsf in Hole 780C and 15.4–32.4 mbsf in Hole 780D) comprises intervals of serpentinitized ultramafic rocks in a matrix of sandy silt- and clayey silt-sized serpentine.

The mineralogy of the clasts and serpentine-rich matrix is similar to that of the materials from the flank sites (Sites 778 and 779), except that the matrix contains delicate aragonite needles indicative of authigenic growth after the serpentine was emplaced. In terms of structure, however, the matrix, though chaotic, typically lacks the foliation and shear fabric seen in the matrix from the flank sites. Therefore, this matrix may be interpreted as upwelling serpentinite, upon which foliation and shear fabric have been imposed by compaction, extension, and pure shear during the downhill creep of serpentinite debris flows. Studies of physical properties give a density range of 1.75 to 2.0 g/cm³ and compressional-wave velocities of 1.5 to 2 km/s for this serpentine-rich matrix and together with rheological measurements indicate that it is a weak, highly non-ideal, plastic material capable of supporting blocks up to 20 m wide.

Analyses of interstitial pore-water samples at Site 780 revealed marked downhole chemical changes, including an increase in alkalinity from 2.5 to 34 and in pH from about 8 to 12.4, together with major depletions in calcium and magnesium; increases in sulfate, potassium, and ammonia; and decreases in salinity and chlorinity. These changes take place within a few meters of the seafloor, showing that the fluid entrained within the serpentinite may only mix with seawater at shallow levels. The magnitude and direction of these changes also differ in significant ways compared to the flank sites, revealing major variability in fluid chemistry and fluid flow within the seamount.

BACKGROUND AND SCIENTIFIC OBJECTIVES

The summit of Conical Seamount, where Site 780 is located, lies at a depth of about 3100 m (Fig. 1). SeaMARC II side-scanning sonar images of this summit revealed recent flows of unconsolidated sedimentary serpentinite, apparently emanating from and mantling the summit region. Thus, we inferred that the summit region of the seamount might be the site of emanations of recent, diapirically emplaced serpentinite flows (Fryer et al., 1987; Fryer et al., this volume). Results of *Alvin* dive studies of the seamount summit showed that fluids are actively seeping from chimneys and related structures on the west side of the southern summit knoll (Fig. 2). These fluids are precipitating carbonate and silicate compounds that form the chimneys and cement the uppermost portion of the sedimentary serpentinite flows (Fryer et al., 1987). At no other locality on the seamount that was explored with the *Alvin* submersible, or subsequently surveyed with bottom video or still photography (P. Stoffers, pers. comm., 1989), were active seeps or chimney structures observed. The southwestern side of the summit of Conical Seamount therefore provides a locality for studying the active formation of sedimentary serpentinite flows and their associated fluids and mineral deposits.

Drilling at Site 780 was undertaken to enable us to investigate (1) the mechanical properties of the diapiric neck and emplacement mechanism of the diapir, (2) the composition of the associated fluids and entrained metamorphosed xenoliths, (3) the compositional and physical variability of the rising diapiric material, and (4) the potential for ore deposition within serpentinite diapirs. While these immediate objectives are site specific, they apply to the understanding of several larger questions. The most obvious of these are both the relationship of diapirism to the history of development of the forearc region of an intraoceanic arc system and the geochemical mass balance of the subduction process.

The physical properties of the diapir and the mechanism of its emplacement can be studied in greatest detail at Site 780. Here, strong evidence suggests that the rising serpentinite diapir entrains deep-seated fluids as it rises and loses these fluids during protrusion of the serpentine flows onto the surface (Fryer et al., 1987; Haggerty, 1987a, 1987b; Fryer et al., this volume). Strong evidence exists for compaction of these flows soon after they are erupted, perhaps because of the escape of entrained fluids. Once the rising diapir has stopped erupting and/or stopped venting fluids, the density of the serpentinite may increase. It is also possible that the physical properties of the diapir will change with depth as well as with age. Documenting such changes and the study of the physical properties of the diapiric material will permit better interpretation of sedimentary serpentinite deposits in sub-aerial exposures, such as those of the basal Great Valley sequence in Napa County, California (Phipps, 1984). Studies of the composition of fluids collected with the *Alvin* from an actively seeping chimney structure on Conical Seamount (Fryer et al., this volume) have revealed high pH (9.28 vs. 7.72 for ambient seawater), high alkalinity (5.53 vs. 2.41 meq/L) and enrichment in CH₄ (1000 vs. 2.1 nM), SiO₂ (0.75 vs. 0.12 mM), SO₄ (30.4 vs. 28.6 mM), and H₂S (2.1 nM vs. not detected) (B. Tilbrook, pers. comm., 1988). The CH₄ and H₂S detected in the vent fluids were particularly interesting. Because the Mariana forearc has only a small volume of sedimentary substrate (Hussong and Uyeda, 1981), with organic carbon contents typically less than 0.3% (Schorno, 1981), the methane and sulfide in the Mariana vent fluids are unlikely to have formed by the biogenic processes associated with accretionary complexes (Kulm et al., 1986). Rather, they were probably generated during serpentinitization reactions. Overall, the chemical analyses of these fluids imply that deep-seated serpentinitization processes, juvenile mantle fluids, interaction of seawater with crustal rocks, and interactions of seawater with the surficial serpentinite may all contribute to the composition of the fluids.

Compositions of trace element and stable isotopes of the carbonate chimney materials from Conical Seamount are also consistent with deposition from serpentinite-related fluids, which contained components from either the forearc mantle or the subducted slab or both (Haggerty, 1987a). Compared with carbonates of the fracture zone thought to have a dominantly seawater origin, for example, Mariana aragonite is depleted in strontium (Mariana samples = 7,000–9,400 ppm; fracture-zone aragonite = 9,500–11,600 ppm), enriched in magnesium (Mariana = 750–6,300 <300 ppm, fracture zone, <300 ppm), and has a significantly lighter carbon isotopic signature (Mariana = -1.2 to -21.2‰, fracture zone = +0.03 to +1.12‰) and heavier oxygen isotopic signature (Mariana = +5.1 to +7.6‰, fracture zone = +3.16 to +4.87‰). These values are consistent with both an origin involving seawater interactions with ultramafic rocks and an origin involving derivation from dewatering of subducted oceanic lithosphere and/or from the

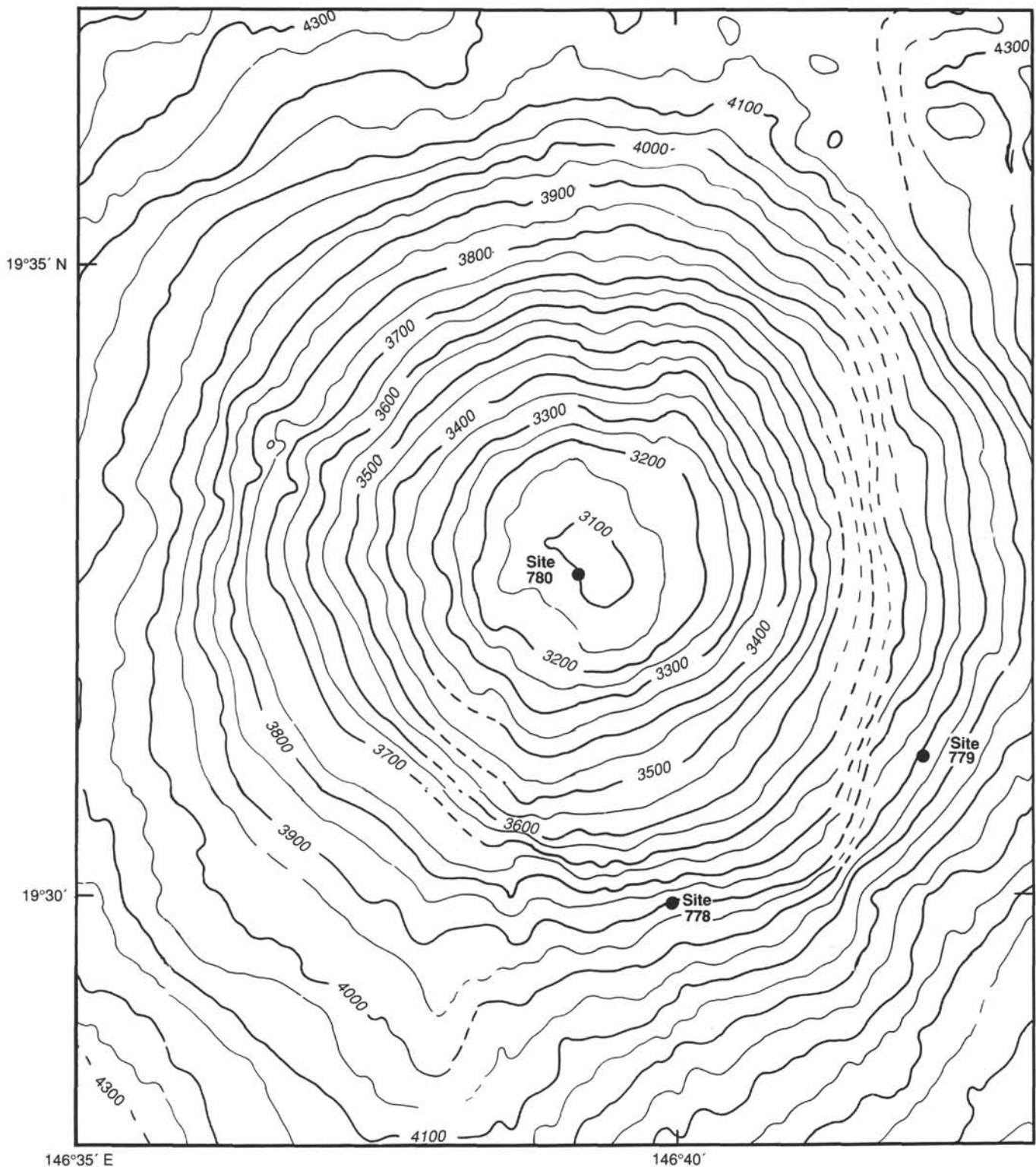


Figure 1. SeaBeam bathymetric contour map (in meters) of the upper flanks of Conical Seamount, showing the positions of Sites 778, 779, and 780.

mantle underlying the forearc. Detailed sampling at depth within the serpentinite body should constrain either the nature of the shallow level reactions influencing the fluid composition or the possible sources of the fluids.

Several sedimentary serpentinite deposits on land have yielded ore-grade deposits of a variety of compounds, nota-

bly nickel/iron, mercury, chromium, and native gold. The nature of these deposits depends on the local oxidation-reduction conditions of the rising diapir. By drilling, we hoped to secure samples that would allow us to constrain the small-scale variations in conditions of fluids within the serpentinite.

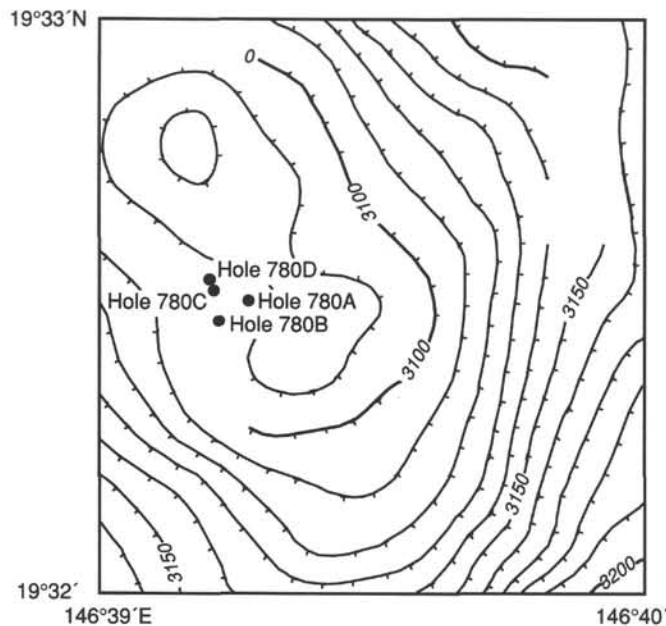


Figure 2. Detailed SeaBeam bathymetry map of the summit of Conical Seamount, showing the positions of Holes 780A through 780D.

OPERATIONS

Transit to Site 780 (MAR-3A)

Although Site 780 is located on the summit of Conical Seamount, 2.5 nmi from Site 779, a seismic survey was required to determine its exact location. The survey began during a GPS window at 1715 hr UTC (Universal Time Coordinated), 3 March. Site 780 was established by dropping a beacon at 2245UTC, 3 March.

HOLE 780A

A standard APC/XCB bottom-hole assembly (BHA) was prepared with a soft-formation bit and lockable flapper valve (LFV). The trip in began at 0030UTC, 4 March, when the drill bit was lowered through the drill floor. A small area was targeted for drilling, and the television camera was lowered to scan the seafloor for the best spud site. At 0845UTC, 4 March, Hole 780A was spudded with the APC. The water depth was determined (as 3086.8 mbsl) by observing the drill string tag the seafloor.

Unfortunately, the APC core barrel bent on impact when the first APC was shot. Efforts to retrieve the core barrel proved futile. The drill string was manipulated in an attempt to break off the bent core barrel so that the hole could be continued with the XCB and the pressure core sampler (PCS). During this procedure, the television cable became tangled in the drill string and/or at the moon pool doors, causing the cable to fail in the moon pool area. The vibration-isolated television (VIT) frame with the television camera and 3100 m of cable were lost. The drill string was tripped out slowly in the hope that the fouled cable and bent core barrel would retain the VIT. When the BHA was pulled into the moon pool, however, only the bent core barrel was found. Hole 780A officially ended when the bit was back on deck at 1830UTC, 4 March. The APC was deployed once to a depth of 3.5 mbsf, where we recovered 3.54 m of core for a recovery rate of 101% (Table 1).

HOLE 780B

The vessel was offset 100 m west, and a standard RCB BHA was prepared with a soft-formation bit and mechanical

Table 1. Coring summary for Site 780.

Core no.	Date (Mar. 1989)	Time (UTC)	Depth (mbsf)	Length cored (m)	Length recovered (m)	Recovery (%)
125-780A-1H	4	1845	0-3.5	3.5	3.54	101.0
Coring totals				3.5	3.54	101.0
125-780B-1R	5	0755	0-8.7	8.7	8.75	100.0
2R	5	0915	8.7-18.2	9.5	1.59	16.7
Coring totals				18.2	10.34	56.8
125-780C-1R	6	0450	0-5.5	5.5	5.49	99.8
2R	6	0545	5.5-14.0	8.5	0.56	6.6
3R	6	0820	14.0-23.5	9.5	0.59	6.2
4R	6	0940	23.5-33.0	9.5	0.26	2.7
5R	6	1110	33.0-42.5	9.5	0.67	7.1
6R	6	1330	42.5-52.1	9.6	0.85	8.9
7R	6	1510	52.1-61.5	9.4	0.26	2.8
8R	6	1820	61.5-71.1	9.6	1.15	12.0
9R	6	2020	71.1-80.8	9.7	0.57	5.9
10R	6	2200	80.8-90.5	9.7	0.27	2.8
11R	6	2300	90.5-100.2	9.7	0.07	0.7
12R	7	0200	100.2-106.5	6.3	0.38	6.0
13R	7	0400	106.5-116.0	9.5	0.67	7.1
14R	7	0530	116.0-125.5	9.5	0.09	1.0
15R	7	0650	125.5-135.0	9.5	0.62	6.5
16R	7	0815	135.0-144.6	9.6	0.48	5.0
17R	7	0950	144.6-154.0	9.4	0.06	0.6
18R	7	1515	154.0-163.5	9.5	1.40	14.7
Coring totals				163.5	14.44	8.8
125-780D-1X	8	0800	0-2.5	2.5	2.50	100.0
2X	8	0910	2.5-12.0	9.5	1.51	15.9
3X	8	1015	12.0-15.4	3.4	0.31	9.1
4C	8	1825	15.4-16.9	1.5	0.00	0.0
5X	8	2100	16.9-20.4	3.5	0.16	4.6
6X	9	0030	20.4-27.4	7.0	1.29	18.4
7X	9	0330	27.4-32.4	5.0	3.32	66.4
Coring totals				32.4	9.09	28.1

bit release (MBR). Hole 780B was spudded at 0530UTC, 5 March. The first core barrel retrieved had a shattered liner, which required us to respud the hole. Hole 780B was respudded at 0645UTC, 5 March, establishing the mud line at 3094.0 mbsl with the first core.

The sinker-bar assembly was lost during our attempt to retrieve Core 125-780B-3R. Apparently, the bit had followed the slope of a hard serpentinite layer, causing part of the BHA to break off. The drill string was tripped out, and Hole 780B officially ended at 1900UTC, 5 March. Two successful cores were recovered from Hole 780B to a total depth of 18.2 mbsf using the RCB. A total of 10.34 m of core was recovered for a recovery rate of 57% (Table 1).

HOLE 780C

The *Resolution* was offset 50 m north. Another standard RCB BHA was prepared and tripped to the seafloor. Hole 780C was spudded at 1900UTC, 5 March. The mud line was established at 3083.4 mbsl with recovery of the first core. The hard serpentinite present in Hole 780B was encountered at 14 mbsf in Hole 780C and was penetrated after rotation of 1.75 hr. Drilling continued, but with considerable difficulty. At a total depth of 163.5 mbsf, the hole finally collapsed, and 20 m of hole was lost.

The shipboard scientific party hoped to log the hole. Although hole conditions were not favorable, the bit was released and the logging line prepared. The first and second logging runs were aborted because of problems with the cable head. By the time the logging tools reached the open hole, the hole had closed in, curtailing the logging. A temperature profile was the only result of the logging effort.

A total of 18 RCB cores were taken from Hole 780C, recovering 14.44 m of core for a recovery of 9% (Table 1). Hole 780C officially ended with the BHA back on deck at 1830UTC, 8 March.

HOLE 780D

Because of the poor recovery in Hole 780C, the vessel was offset 50 m northwest and, using the new XCB (Leg 124E), Hole 780D was spudded at 0100UTC, 9 March. During retrieval of the first core barrel, at 1100 m below the dual elevator stool (DES), the sand line parted approximately 25 m above the sinker-bar assembly. When finally recovered, the core barrel was empty.

Hole 780D was spudded at 0700UTC, 9 March, and the first core established the mud line at 3088.9 mbsl. A hard serpentinite layer was encountered at 16.9 mbsf, where 7.5 hr of rotation was required to penetrate it. A standard carbide-tooth center bit was used to drill the first meter of the 1.5-m-thick layer. An impregnated diamond cutting shoe was installed on an XCB core barrel and deployed. Penetration rates increased noticeably, and a small core of the serpentinite was recovered.

After penetrating the hard serpentinite layer, the water sampler temperature probe (WSTP) was deployed at a depth of 20.4 mbsf. The water sampler valve failed to open, but temperature data were obtained. The WSTP was deployed again at 27.4 mbsf and at 41.8 mbsf. The second deployment recovered a water sample, but no temperature data. The third deployment resulted in the acquisition of both a water sample and temperature data.

Hole 780D and Site 780 were abandoned at the request of the Co-Chief Scientists and officially ended at 1345UTC, 10 March, when the bit was back on deck. The XCB was deployed six times in Hole 780D, which resulted in 32.4 m cored, and core recovery of 9.1 m for a recovery rate of 28.1% (Table 1). Drilling produced another 10.9 m of penetration to a total depth of 41.8 mbsf.

LITHOSTRATIGRAPHY

Lithologic Summary

At Site 780, four holes were drilled within 163 m of each other into the summit of Conical Seamount. The stratigraphic section at Site 780 has been divided into two lithologic units: lithologic Unit I of sand- and silt-sized serpentine, with intervals of foraminifer-rich serpentine clay and serpentine-

rich clayey silt; and lithologic Unit II of serpentinized harzburgite and subordinate serpentinized dunite in a serpentine matrix (for a description of the metamorphosed rocks, see "Igneous and Metamorphic Petrology" section, this chapter). These units, their sub-bottom depths, and biostratigraphic ages are summarized in Table 2.

Unit I

Sections 125-780A-1H-1, 0 cm, to 125-780A-1H-1-CC; depth, 0–3.5 mbsf; Sections 125-780B-1R-1, 0 cm, to 125-780B-2R-CC; depth, 0–18.2 mbsf; Sections 125-780C-1R-1, 0 cm, to 125-780C-2R-CC; depth, 0–14 mbsf; Sections 125-780D-1X-1, 0 cm, to 125-780D-3X-CC; depth 0–15.4 mbsf.

This unit extends from the sediment/water interface to a maximum depth of 18.2 mbsf and is primarily a multicolored sand- and silt-sized serpentine, with sand- to pebble-sized clasts of serpentinite and other lithic types. Filamentous opaque mineral aggregates (interpreted as remnants of bacterial mats) were found in smear slides throughout this unit.

Calcareous nannofossils identified in Sample 125-780C-2R-CC are middle to late Pleistocene in age. The uppermost section of the first core (material associated with the present surface of the seafloor) was not sampled for biostratigraphic dating from the majority of holes on this leg. Therefore, the age of that sediment associated with the top of these holes has been inferred as Holocene. This inference at Site 780 is supported by the biostratigraphic age determined for Sample 125-780D-1X-1, 6 cm, which is of late Pleistocene age on the basis of the nannofossil assemblage. The age of the base of the unit is unknown. A middle to late Pleistocene age was obtained from nannofossil assemblages in Samples 125-780A-1H-CC; 125-780B-1R-3, 11 cm; 125-780C-1R-2, 112 cm; 125-780C-1R-3, 81–83 cm; 125-780C-1R-CC; and 125-780C-2R-CC. Sediments in all remaining core-catcher samples from beneath the above-listed samples from Unit I are barren; the unit can thus be inferred to be at least middle Pleistocene in age and may be older (see "Biostratigraphy" section, this chapter).

Dark green (5B 4/1 to 5G 7/2) and black (7.5YR 2/0), angular to rounded clasts of serpentinite, ranging in size from 1 mm to 5 cm, are scattered throughout the multicolored sand- and silt-sized serpentine in Unit I. Overall, the color of the unit is predominantly bluish gray (5B 4/1 to 7/1). A multicolored appearance results from the presence of light olive gray (5Y 5/2), brown (10YR 5/3), and dark gray (7.5YR 4/0) intervals, mottled with

Table 2. Lithologic units recovered at Site 780, Leg 125.

Lithologic unit/subunit	Cores	Depth (mbsf)	Dominant lithology	Stratigraphic age	
I	125-780A-1H-1, 0 cm to 125-780A-1H-CC	0–3.5	Sand-, and silt-sized serpentine with some intervals aragonite-rich;	Holocene(?) to middle Pleistocene(?)	
	125-780B-1R-1, 0 cm to 125-780B-2R-CC	0–18.2	rare intervals of foraminifer-rich serpentine clay, and serpentine-rich silty clay.		
	125-780C-1R-1, 0 cm to 125-780C-2R-CC	0–14.0			
	125-780D-1X-1, 0 cm to 125-780D-3X-CC	0–15.4			
	II	125-780C-3R-1, 0 cm to 125-780C-18R-CC	14.0–163.5	Intervals of serpentinized harzburgite and dunite in a	(?)
		125-780D-4X-1, 0 cm to 125-780D-7X-CC	15.4–32.4	matrix of sandy silt, and clayey silt-sized serpentine	

dusky blue (5PB 3/2), pale yellow (5Y 8/3), or light green (5G 7/2). The unit has been variably disturbed by drilling, which enhances the mottled appearance. Color variations are not reflected in the composition of the multicolored serpentine, which is 75% to 98% serpentine, 3% to 20% opaque minerals, 0% to 20% aragonite, 0% to 10% zoisite, 2% to 10% chlorite, and up to a trace of amphibole, garnet, and epidote.

Most of the serpentine matrix lacks biogenic and detrital components, but does contain authigenic aragonite needles. An exception is the material recovered in the APC core (Core 125-780A-1H) from Hole 780A, where aragonite crystals are found only in the serpentine clay containing trace amounts of foraminifers, nannofossils, radiolarians, and silicoflagellates (Sample 125-780A-1H-CC). The presence of acicular aragonite crystals is characteristic of the matrix of Unit I, in which the acicular aragonite sometimes forms a mesh that gives a firm or stiff texture to the serpentine. No obvious structures of primary sedimentary origin are present. All structures are indicative of tectonic deformation (see "Structural Studies" section, this chapter).

Unit I also contains some sediments that have an obvious biogenic and detrital component. There are foraminifer-bearing serpentine silts and clays that contain serpentine (68%–76%), opaque minerals (5%–10%), aragonite (5%–6%), foraminifers (10%), nannofossils (1%–2%), spicules (0%–3%), silicoflagellates (1%–2%), diatoms (1%), and radiolarians (0%–1%) (in Samples 125-780B-1R-1, 77 cm; 125-780D-1X-2, 2 cm), as well as serpentine clay that contains clay (20%), serpentine (55%), chlorite (trace), opaque minerals (20%), and zoisite (5%). Where the opaque minerals are abundant in smear slides, they are present as filamentous opaque mineral aggregates that may be a remnant of a bacterial mat (for example, Sample 125-780A-1H-CC). Intercalations of these sediments containing pelagic detritus indicate periods of multiple exposure of serpentine at the seafloor.

Aragonite near the sediment/water interface is unusual at this water depth (Haggerty, 1980), as noted also for Sites 778 and 779, because seawater below a few hundred meters in the present-day Pacific Ocean is undersaturated with respect to aragonite (Li et al., 1969; Berner and Honjo, 1981), and because the aragonite compensation depth is less than 1000 mbsl throughout the Pacific, often as shallow as 400 mbsl (Berger, 1970). The presence of aragonite crystals in the clay and serpentine thus implies authigenic growth after serpentine emplacement and flow.

On the basis of similar lithologies and biostratigraphic criteria, this unit correlates with Unit I at Sites 778 and 779. This assumption may not be valid if the flank site drill holes are through serpentine flows and if the summit holes are through *in-situ* serpentine.

Unit II

Sections 125-780C-3R-1, 0 cm, to 125-780C-18R-CC; depth, 14–163.5 mbsf; Sections 125-780D-4X-1, 0 cm, to 125-780D-7X-CC; depth, 15.4–32.4 mbsf.

Lithologic Unit II contains intervals of serpentized harzburgite and serpentized dunite (see "Igneous and Metamorphic Petrology" section, this chapter) in a serpentine matrix. This matrix is bluish gray (5B 5/1) to greenish gray (5BG 5/1 and 6/1) and contains serpentinite clasts ranging from 1 mm to 1 cm in size. The matrix is clayey silt-sized serpentine composed of 70% to 99% serpentine, 1% to 15% opaque minerals, 0% to 10% clay, 0% to 5% zoisite, 0% to trace amounts of thulite, 0% to 5% chlorite, with up to 2% micrite and garnet. The matrix has been highly deformed by drilling.

BIOSTRATIGRAPHY

Calcareous nannofossil and planktonic foraminiferal evidence indicates that the upper portions of the sediments in Holes 780A, 780B, 780C, and 780D range in age from middle to late Pleistocene. A sediment interval in Sample 125-780D-6X-1, 34–40 cm, was dated as Pleistocene; poor preservation of the extracted foraminiferal assemblage did not allow us to refine this age.

Calcareous Nannofossils

Hole 780A

Nannofossils are present in only one sample in Hole 780A (125-780A-1H-CC). This sample contains a common, well-preserved assemblage characterized by the following species: *Emiliania huxleyi*, *Gephyrocapsa oceanica*, *Calcidiscus leptoporus*, *Helicosphaera carteri*, *Oolithothus fragilis*, *Ceratolithus cristatus*, *Ceratolithus telesmus*, *Rhabdosphaera clavigera*, and *Hayaster perplexus*. The absence of *Calcidiscus macintyreii* and *Pseudoemiliania lacunosa* and the presence of *Emiliania huxleyi* confine this sample to the late Pleistocene (Zone CN15).

Hole 780B

A rare, well-preserved coccolith assemblage was found in Sample 125-780B-1R-3, 11 cm. The presence of *Emiliania huxleyi*, *Cricolithus jonesi*, *Gephyrocapsa oceanica*, *G. caribbeanica*, *Helicosphaera wallichii* and *Ceratolithus cristatus* allows the designation of a late Pleistocene age (Zone CN15).

Hole 780C

Moderately to well-preserved, few to common, Pleistocene nannofossil assemblages are present in Samples 125-780C-1R-2, 112 cm; 125-780C-1R-3, 81–83 cm; 125-780C-1R-CC; and 125-780C-2R-CC. These four samples contain similar assemblages that are characterized by *Gephyrocapsa oceanica*, *Calcidiscus leptoporus*, *Umbilicosphaera mirabilis*, *Oolithothus fragilis*, *Umbellosphaera irregularis*, *Scapholithus fossilis* and *Helicosphaera carteri*, but lack *Helicosphaera sellii* and *Calcidiscus macintyreii*. We assigned this assemblage to the middle to late Pleistocene (Zones CN14b to CN15) based on Okada and Bukry (1980) and Backman, Duncan, et al. (1988).

Hole 780D

Only three samples (125-780D-1X-1, 6 cm; 125-780D-2X-CC; and 125-780D-6X-1, 34–40 cm) contain nannofossils. A diverse, well-preserved assemblage in Sample 125-780D-1X-1, 6 cm, includes common *Gephyrocapsa caribbeanica*, *Umbellosphaera irregularis*, *Helicosphaera hyalina*, *Calcidiscus leptoporus* and *Gephyrocapsa oceanica*. This assemblage may be assigned to the late Pleistocene (Zone CN15). In the two other samples (125-780D-2X-CC and 125-780D-6X-1, 34–40 cm), we found a rare, poorly preserved nannofossil assemblage. This assemblage contains *Umbellosphaera irregularis*, *Calcidiscus leptoporus*, *Gephyrocapsa oceanica* and *Helicosphaera* sp. These samples may be assigned to the Pleistocene (Zone CN14 to CN15).

Foraminifers

Pleistocene (Zone N22) planktonic foraminiferal assemblages of moderate preservation were recovered from Samples 125-780A-1H-CC and 125-780C-1R-CC. Both samples contain *Globorotalia truncatulinoides* and are dominated by *Globigerinoides conglobatus*, *G. immaturus* and *Globorotalia menardii*.

Samples 125-780C-1R-3, 81–83 cm, and 125-780D-1X-CC yielded sparse, moderately preserved planktonic foraminiferal assemblages that can be assigned an age of late to early Pliocene to Pleistocene (Zones 19/20 to 22); the absence of diagnostic species precludes a more precise age determination. Both samples contain abundant *G. immaturus* and *G. conglobatus*. We did not find any foraminifers in Hole 780B.

In all samples examined, we noted a conspicuous lack of benthic foraminifers. This absence (of both calcareous and agglutinated forms) may be a result of adverse sediment conditions.

Diatoms

Rare, moderately preserved diatoms (mostly as fragments) were observed in Samples 125-780A-1H-CC and 125-780C-2R-CC only. We were unable to determine an age on the basis of the observed diatoms.

Radiolarians were observed in the above samples and in Sample 125-780B-1R-CC.

IGNEOUS AND METAMORPHIC PETROLOGY

The hard rocks recovered at Site 780 are variably serpentinized and tectonized ultramafic rocks, together with three sedimentary clasts. Of the ultramafic rocks, about 90% are harzburgite and 10% are dunite. Two of the sedimentary clasts are weak red (5R 5/2) siltstone with carbonate veins, and one is greenish white (5Y 8/1) carbonate. The ultramafic clasts reach a maximum recovered thickness of about 1.2 m (Section 125-780C-18R-1) and are enclosed in a sheared and deformed serpentinite matrix that is described in the "Structural Studies" section (this chapter). Contacts between the ultramafic and sedimentary rocks are ambiguous.

Ultramafic Rocks

Serpentinized and Tectonized Harzburgites

The harzburgites are massive and vary from gray (10Y 5/1), where relatively fresh, to bluish gray (5B 4/1), where serpentinized (e.g., Interval 125-780C-18R-1, 36–45 cm, and 25–36 cm, respectively; Fig. 3). The primary mineralogy of these rocks is olivine (75%–90%), orthopyroxene (10%–25%), chromium-spinel (trace to 2%), and clinopyroxene (trace to 2%). Clinopyroxene is present as blebs and anhedral crystals (<1 mm), typically closely related to orthopyroxene, and as exsolution lamellae (on [100]) in orthopyroxene.

The harzburgites display penetrative deformation. Typically, orthopyroxene crystals are 1 to 4 mm in size and have morphologies that range from equant to asymmetric-elongate; cleavage surfaces and extinction are wavy, kink-banding is common, and fine clinopyroxene exsolution lamellae on (100) are bent. Elongate crystals (<5 mm long) and kink-banding (sometimes showing fine lamellae) characterize some of the olivine morphologies. Microgranular (<0.5 mm equant crystals) fabrics indicative of recrystallization under relatively high temperature are also present. Chromium-spinel crystals range from equant (0.5 mm in size) to elongated shapes (up to 2 mm long). Some of the elongate spinels define a lineation parallel to the elongate olivine and orthopyroxene (see "Structural Studies" section, this chapter).

The degree of serpentinization is extremely variable (50%–100%), with the olivine and orthopyroxene replaced by mesh-textured serpentine (chrysotile-rich) and bastite, respectively. In these strongly serpentinized types, most of the chromium-spinel (translucent, shades of red) is fresh. Antigorite and brucite may also be present. The harzburgites are cut by numerous veins of serpentine. Many of these veins show a polystage history of filling. Typically, serpentinization affects

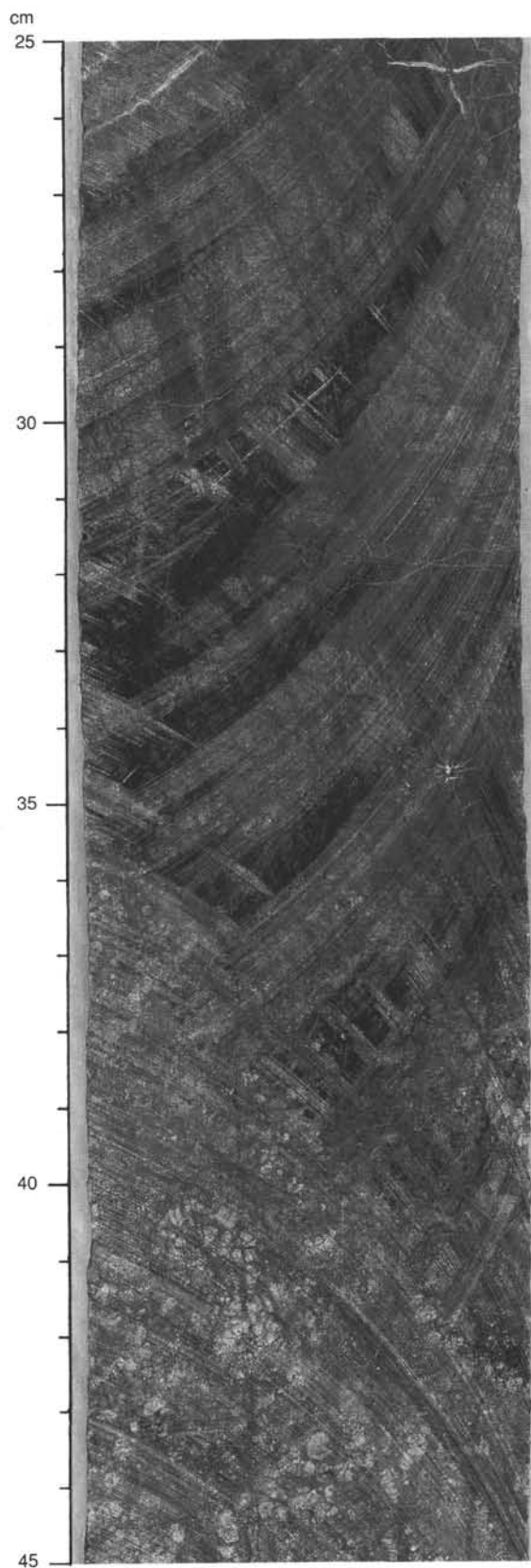


Figure 3. Interval 125-780C-18R-1, 25–45 cm. Harzburgite containing relatively fresh (36–45 cm) and serpentinized (25–36 cm) areas.



Figure 4. Interval 125-780B-1R-CC, 0–10 cm. Altered clay-rich (brecciated?) siltstone with white carbonate veins, contacting soft sediments.

olivine the most, orthopyroxene less, and clinopyroxene and chromium-spinel the least in this site. Subhedral primary clinopyroxenes (<0.5 mm long) were observed in some samples.

Serpentinized and Tectonized Dunites

These rocks are greenish dark gray (5Y 2.5/1), are generally massive, and sometimes grade to harzburgite. The primary mineralogy consists of olivine (90%–99%), orthopyroxene (1%–9%), and spinel (trace to 1%). Most dunites are exten-



Figure 5. Interval 125-780C-12R-1, 23–30 cm. Altered clay-rich siltstone (5R 5/2; weak red in color) with white carbonate veins.

sively (90%–100%) serpentinized and show mesh textures, splays of chrysotile, and are cut by numerous serpentine-rich veins. Some dunites are rich in antigorite and brucite. Microgranulation of relict olivine, kink-banding of orthopyroxene and olivine, and asymmetric elongation of spinel are evidence of penetrative deformation. Other secondary minerals include magnetite, which replaces chromium-spinel and is found in serpentine veins, and up to 5% chlorite, clays (after serpentine) and talc.

Table 3. Tabulated major-element data for serpentinized, ultramafic rocks from Site 789.

Hole:	Harzburgites					Average harzburgites	Dunite 780C 8R-1 98–101
	780C 6R-1	780C 10R-1	780C 16R-1	780C 18R-1	780C 18R-1		
Core:	6R-1	10R-1	16R-1	18R-1	18R-1		
Interval (cm):	61–62	13–16	53–59	54–57	58–61		
SiO ₂	40.70	38.42	37.76	38.56	38.85	38.86	38.43
TiO ₂	0.00	0.00	0.00	0.00	0.00	0.00	0.00
Al ₂ O ₃	0.47	0.60	0.54	0.63	0.66	0.58	0.65
Fe ₂ O ₃	7.91	7.45	7.44	7.80	7.81	7.68	7.84
MnO	0.11	0.11	0.11	0.11	0.11	0.11	0.11
MgO	42.94	39.04	39.97	39.13	38.87	39.99	39.78
CaO	0.60	0.79	0.69	0.86	0.89	0.77	0.50
Na ₂ O	0.00	0.00	0.00	0.00	0.00	0.00	0.00
K ₂ O	0.00	0.02	0.01	0.00	0.00	0.01	0.01
P ₂ O ₅	0.00	0.00	0.03	0.00	0.00	0.01	0.00
NiO	0.29	0.28	0.29	0.29	0.28	0.29	0.29
Cr ₂ O	30.24	0.31	0.31	0.28	0.34	0.30	0.34
LOI	5.28	12.31	12.06	11.13	11.12	10.38	11.90
Total	98.55	99.31	98.60	98.78	98.92	98.83	99.84
Mg#	91.49	91.21	91.41	90.86	90.79	91.16	90.95
% SERP	65	65	70	75	75	70	55

Data (in wt%) are from whole-rock analyses by XRF. LOI = loss on ignition between 150°C and 1030°C; % SERP = percentage of serpentinization as estimated from thin sections.

Sedimentary Rocks

Of the two sedimentary clasts, one is included in the soft sediments (Interval 125-780B-1R-CC, 0–10 cm; Fig. 4) and the other is isolated (Interval 125-780C-12R-1, 23–30 cm; Fig. 5). Both clasts may be altered clay-rich siltstones, and include microfossils (foraminifers and radiolarians) and white carbonate veins (Figs. 4 and 5). The greenish white clast in Figure 5 is a calcite fragment (about 5 cm) that also includes microfossils (radiolarians).

IGNEOUS AND METAMORPHIC GEOCHEMISTRY

Six of the ultramafic clasts (five harzburgite, one dunite) from Site 780 were selected for shipboard geochemical analysis. Rock descriptions can be found in the "Igneous and Metamorphic Petrology" section (this chapter) and preparation and analytical techniques in the "Explanatory Notes" (this volume). Geochemical data are listed in Tables 3 and 4.

Ultramafic Samples

Modal estimates of the original (pre-serpentinization) composition of ultramafic rocks range from 5% to 25% orthopyroxene, 75% to 95% olivine, and <1% clinopyroxene and spinel. All samples are variably serpentinized (55%–75%) and most are tectonized. The compositions of the ultramafic rocks are remarkably similar (Tables 3 and 4) and deviate little from average harzburgite values.

Chemistry of Major Elements

Loss on ignition (LOI) of these samples ranges from 5.28 to 12.31 wt% and, unlike data from Sites 778 and 779, does not correlate with percentage of serpentinization. (See "Igneous and Metamorphic Geochemistry" sections, Sites 778 and 779, and "Explanatory Notes," this volume, for an explanation of LOI.) Concentrations of oxides of major elements (Table 3) are similar in the single dunite sample (125-780C-8R-1, 98–101 cm) and the harzburgites. SiO₂ ranges from 37.76 to 40.70 wt%, and MgO ranges from 39.13 to 42.94 wt%. Several poorly constrained trends can be seen in co-variation plots of the data (Figs. 6A and 6B), but we cannot be certain that these trends are real and not an artifact of a small data set (six samples). Both SiO₂ and MgO are inversely correlated with LOI. Al₂O₃ ranges from 0.47 to 0.65 wt%, and Fe₂O₃ ranges from 7.44 to 7.91 wt%. The magnesium number (Mg# = Mg/(Mg+Fe) × 100) is high, ranging from 90.86 to 91.49. Values of Na₂O, K₂O, and P₂O₅ are low in all samples; K₂O and P₂O₅ values reach 0.02 and

Table 4. Tabulated trace-element data for serpentinized, ultramafic rocks from Site 780.

Hole:	780C	780C	780C	780C	780C		780C
Core:	6R-1	10R-1	16R-1	18R-1	18R-1	Average	8R-1
Interval (cm):	61–62	13–16	53–59	54–57	58–61	harzburgites	98–101
Nb	tr	tr	tr	tr	tr	tr	tr
Zr	0	1	1	1	1	1	1
Y	nd	0	0	1	1	0	0
Sr	3	9	11	nd	0	5	6
Rb	0	1	1	nd	0	0	0
Zn	33	35	45	33	33	36	32
Cu	3	2	8	10	12	7	1
Ni	2319	2188	2264	2318	2207	2259	2280
Cr	1620	2103	2126	1907	2303	2012	2295
V	25	24	30	25	33	27	41
Ce	nd	nd	tr	nd	tr	tr	nd
14	tr	tr	tr	nd	tr	13	

Data (in ppm) are from whole-rock analyses by XRF; nd = not detected (background count was greater than sample count); tr = below the detection limit (<5 ppm for Nb; <10 ppm for Ba and Ce).

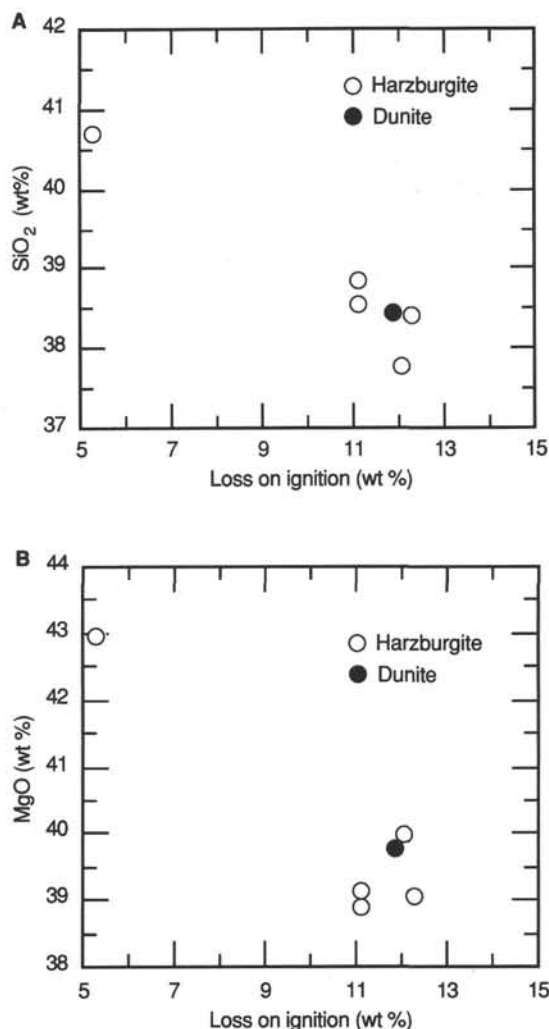


Figure 6. A. Weight percent loss on ignition (LOI) vs. weight percent SiO₂. Data are from Site 780. B. Weight percent loss on ignition (LOI) vs. weight percent MgO. Filled squares represent dunite, and open circles represent harzburgite.

0.03 wt% respectively; and Na₂O values are below the detection limit (<0.01 wt%).

Trace-Element Data

Trace-element data are presented in Table 4. Compatible elements are predictably high in all samples; chromium ranges from 1620 to 2303 ppm, and nickel ranges from 2188 to 2319 ppm. Average concentrations of nickel (harzburgite: 2261 ppm; dunite: 2280 ppm) are slightly lower in samples from Site 780 than for samples from Sites 778 (harzburgite: 2644 ppm) and 779 (harzburgite: 2320 ppm; dunite: 2486 ppm). Chromium and nickel do not correlate with one another or with the degree of serpentinization. Niobium, zirconium, yttrium, rubidium, and titanium are all present at trace levels or are below detection limits. Cesium and barium values typically are below detection limits, although two samples have barium concentrations of greater than 13 ppm. Strontium reaches a maximum of 11 ppm, and vanadium values range from 23 to 41 ppm. Strontium and vanadium concentrations are similar to those in Sites 778 and 779. Zinc values range from 32 to 35 ppm, with a single high concentration of 45 ppm (Sample

Table 5. Total carbon, organic carbon, and carbonate carbon in cores at Site 780.

Core, section, interval (cm)	Depth (mbsf)	Total carbon (%)	Inorganic carbon (%)	Organic carbon (%)	CaCO ₃ (%)
780A-1H-1, 5-6	0.05		0.10		0.8
780A-1H-1, 19-20	0.19		0.12		1.0
780A-1H-1, 39-41	0.39		0.14		1.2
780A-1H-1, 58-60	0.58		0.11		0.9
780A-1H-1, 132-133	1.32		0.05		0.4
780A-1H-2, 68-70	2.18	0.32	0.07	0.25	0.6
780A-1H-CC, 23-25	3.13		0.10		0.8
780B-1R-1, 99-101	0.99		2.40		20.0
780B-1R-2, 39-41	1.89		0.94		7.8
780B-1R-2, 90-91	2.40		1.03		8.6
780B-1R-3, 30-31	3.30	1.32	1.18	0.14	9.8
780B-1R-4, 49-50	4.99		0.75		6.2
780B-1R-6, 99-100	8.49	0.61	0.43	0.18	3.6
780C-1R-1, 0-1	0.00	2.98	2.42	0.56	20.2
780C-1R-1, 30-31	0.30		1.10		9.2
780C-1R-1, 72-74	0.72		0.61		5.1
780C-1R-2, 27-28	1.31		0.88		7.3
780C-1R-2, 64-66	1.68		0.45		3.7
780C-1R-2, 99-100	2.03	2.53	1.97	0.56	16.4
780C-1R-2, 124-125	2.28		2.03		16.9
780C-1R-2, 126-127	2.30		1.49		12.4
780C-1R-3, 16-17	2.70		0.51		4.3
780C-1R-3, 89-91	3.43	0.41	0.26	0.15	2.2
780C-1R-4, 74-75	4.78	0.44	0.14	0.30	1.2
780C-1R-4, 76-78	4.80		0.24		2.0
780C-2R-1, 30-32	5.80	0.37	0.12	0.25	1.0
780C-4R-1, 13-15	23.63	0.46	0.17	0.29	1.4
780C-5R-1, 41-43	33.41	0.33	0.09	0.24	0.7
780C-7R-1, 10-12	52.20	0.25	0.08	0.17	0.7
780C-15R-1, 23-25	125.73	0.31	0.09	0.22	0.7
780C-15R-CC, 12-14	126.08		0.07		0.6
780D-1X-1, 20-22	0.20	3.78	3.77	0.01	31.4
780D-1X-2, 1-2	0.46		0.87		7.3
780D-1X-2, 52-54	0.97	0.59	0.41	0.18	3.4
780D-1X-2, 95-96	1.40		0.13		1.1
780D-1X-3, 45-47	1.96		0.11		0.9
780D-1X-CC, 11-13	2.40		1.14		9.5
780D-2X-1, 30-32	2.80		0.06		0.5
780D-2X-2, 3-5	3.03	0.39	0.09	0.30	0.7
780D-2X-CC, 4-6	3.82		0.09		0.7
780D-3X-1, 13-15	12.13	0.39	0.07	0.32	0.6
780D-6X-1, 62-64	21.02	0.40	0.09	0.31	0.7
780D-6X-2, 41-43	21.59		0.17		1.4
780D-7X-1, 43-45	27.83	0.33	0.08	0.25	0.7
780D-7X-5, 45-47	28.53	0.31	0.07	0.24	0.6
780D-7X-6, 13-15	29.71		0.07		0.6
780D-7X-CC, 20-22	30.69		0.11		0.9

125-780C-16R-1, 53-59 cm). Zinc averages 36 ppm for harzburgite and 32 ppm for dunite in samples from Site 780, which is slightly lower than the average concentrations for Sites 778 (harzburgite = 42 ppm) and 779 (harzburgite = 39 ppm; dunite = 34 ppm). No significant correlation exists between geochemical parameters and depth below the seafloor.

Samples analyzed from Site 780 are therefore quite similar to those from Sites 778 and 779 (see "Igneous and Metamorphic Geochemistry" sections, "Site 778" and "Site 779" chapters, this volume). The few differences between the chemistry of the three sites are noted above, but could be attributed to the smaller data sets for Sites 778 (10 samples) and 780 (six samples) relative to 779 (32 samples).

SEDIMENT/FLUID GEOCHEMISTRY

Sediment Geochemistry

Cores from Site 780 were analyzed on board the ship for inorganic carbon and for total carbon, nitrogen, and sulfur using the techniques described in the "Explanatory Notes"

(this volume). The organic carbon content was then calculated by difference. These results are presented in Table 5 and in Figures 7 and 8. Most of the unconsolidated serpentine section at Site 780 is poor in carbonate, containing less than 1 wt% CaCO₃. The carbonate-rich layer (up to 8 m thick) that first appeared from 1 to 3 mbsf at Sites 778 and 779 is present at Site 780 as well, although it is more variable here. At the other two sites, this layer contained about 15 wt% CaCO₃, whereas at Site 780, it contains 7 to 31 wt%. In Holes 780C and 780D, there are two layers rather than one, separated by 1 to 2 m of unconsolidated serpentine having a lower carbonate content of 1 to 7 wt%. In Holes 780B, 780C, and 780D, this carbonate-rich layer appears to extend all the way to the seafloor, whereas it is absent in Hole 780A, at least below 0.4 mbsf (Fig. 8). Hole 780A, which was drilled with the hydraulic piston corer, penetrated only 3.5 m, but definitely recovered surficial sediments. From the distribution of this layer at the three sites, it is possible that the upper 1 m to a few meters of serpentine was not recovered in Holes 780B, 780C, and 780D, and that Hole 780A did not penetrate far enough to encounter it. The carbonate enrichment in this layer is in the form of aragonite needles distributed throughout the unconsolidated serpentine. Given the occurrence of this layer at or near the seafloor, it is possible that this carbonate enrichment represents a reaction front, in which Ca²⁺ from the overlying

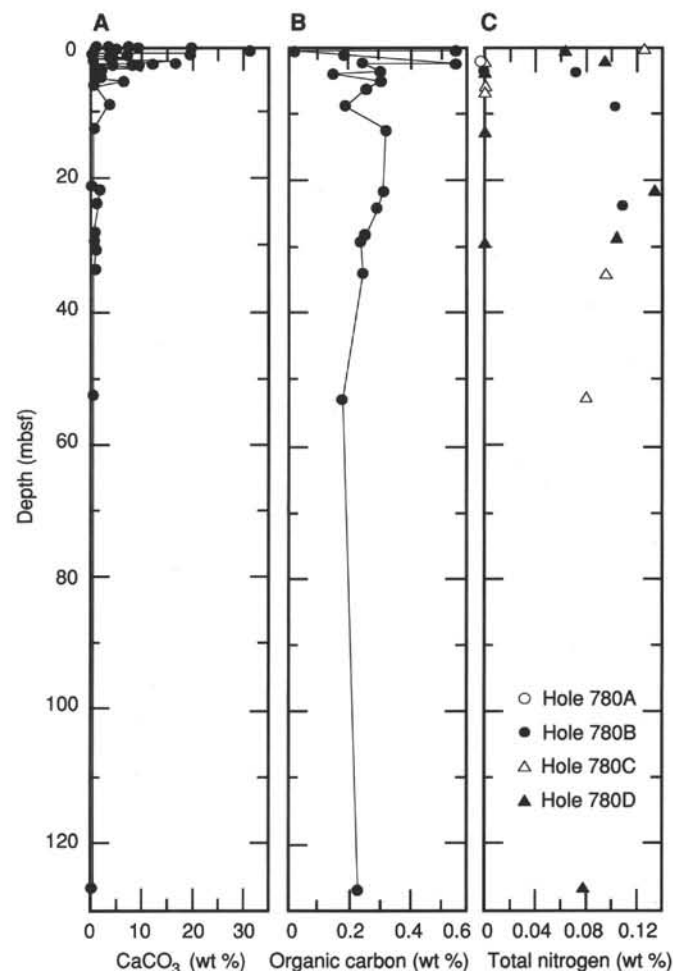


Figure 7. Weight percent of calcium carbonate (A), total organic carbon (B), and total nitrogen (C) in sediments from Holes 780A, 780B, 780C, and 780D.

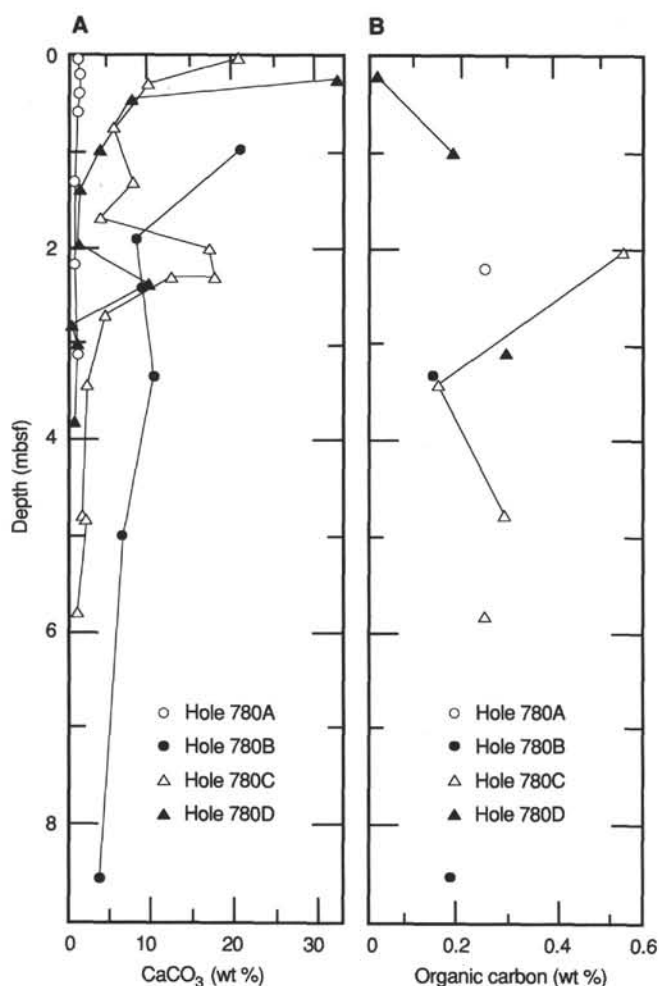


Figure 8. Weight percent of calcium carbonate (A) and total organic carbon (B) in sediments from the upper 9 m at Site 780.

seawater reacts with carbonate ions in the interstitial waters to precipitate authigenic aragonite.

The organic carbon content of the cores at Site 780 (Figs. 7 and 8) varies from 0.01 to 0.56 wt%, in the range of that at Site 779 but higher than that at Site 778. Sulfur ranges up to 0.14 wt%, but was generally not detectable, making Site 780 comparable with Site 779, but sulfur-poor compared with Site 778. Nitrogen ranges up to 0.13 wt%, which is in the same range as values at Sites 778 and 779.

Fluid Geochemistry

Concentrations of methane, ethane, and propane at Site 780 (Tables 6 and 7 and Fig. 9) are as high as those encountered within the upper 156 m of sediment at Site 779 (Fig. 9), and much higher than those at Site 778. Concentrations of these hydrocarbons are very high even in the surficial layer at Site 780; one sample from 1.44 mbsf in Hole 780A yielded 15 mL of methane, 0.1 mL of ethane, and 10 mL of propane per liter of wet unconsolidated serpentine. At the measured porosity of 51% at this depth, this is equivalent to 1.4 mM methane in the interstitial waters. The upper 3 m of serpentine at Site 779 contains low concentrations of hydrocarbons, but we do not know how shallow the high concentrations extend there because the interval between 3 and 43 mbsf could not be sampled. At Site 780, the high concentrations appear to persist to the maximum depth sampled of 126 mbsf, but no samples

Table 6. Results of headspace-gas analyses of cores at Site 780.

Core, section interval (cm)	Depth (mbsf)	Methane ($\mu\text{L/L}$) ^a	Ethane ($\mu\text{L/L}$) ^a	Propane ($\mu\text{L/L}$) ^a	Methane (μM) ^b
125-780A-1H-1, 142-145	1.44	15,229	102	10	1,359
^c 780A-1H-1, 142-145	1.44	12,679	104		1,131
780B-1R-6, 101-106	8.54	18			1.6
780B-2R-1, 145-150	10.18	2,251	50		201
780C-1R-3, 135-140	4.38	9			0.8
780C-4R-1, 20-25	23.73	8,638	41		771
780C-5R-1, 43-48	33.46	31,188	107		2,783
780C-15R-1, 33-38	125.86	22,882	83		2,042
^c 780D-1X-1, 142-145	1.44	177			16
780D-6X-1, 65-68	21.07	13,294	44	4	1,186
780D-7X-5, 125-130	34.68	2,485	11		222

^aMicroliters of gas per liter of wet unconsolidated serpentine.

^bMicromoles of methane per liter of interstitial water, assuming a porosity of 50%.

^cMeasured using Hewlett-Packard gas chromatograph; all others used Carle.

Note: Where values are absent, gas was not detected.

Table 7. Composition of gas pockets in cores from Site 780, sampled through the core liner into an evacuated glass tube.

Core, section, interval (cm)	Depth (mbsf)	Methane (ppmv)	Ethane (ppmv)	Propane (ppmv)
125-780C-18R-1, 25-25	125.75	2809.5	8.3	nd
780D-7X-5, 58-58	33.98	7491.0	28.7	3.0

nd = not detected.

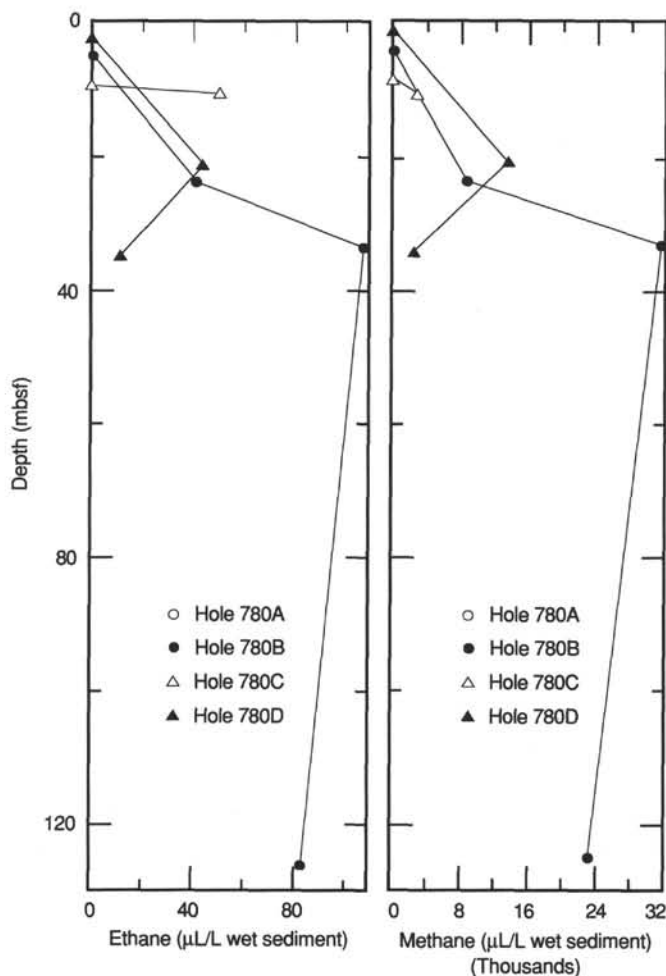


Figure 9. Methane and ethane in cores at Site 780.

Table 8. Composition of interstitial waters from cores at Site 780.

Sample #	Core, section interval (cm)	Volume (mL)	Squeeze T (°C)	Depth (mbsf)	pH	Salinity (R.I., ‰)	Salinity (calc., ‰)	Chlorinity (mmol/kg)	Alkalinity (meq/kg)	Sulfate (mmol/kg)	Sodium (mmol/kg)	Potassium (mmol/kg)	Calcium (mmol/kg)
Surface seawater (4 March 1989)					8.10	35.5	34.85	542.6	2.386	27.98	464.8	10.05	10.17
IW-1	780A-1H-1, 45-55	16	3	0.50	11.37	26.8	29.07	399.0	10.865	32.41	459.6	14.22	0.44
IW-2	780A-1H-1, 95-105	9	3	1.00	11.43	26.5	29.64	393.2	15.042	36.20	464.8	15.21	0.34
IW-3	780A-1H-1, 145-150	33	2	1.48	12.02	25.5	27.21	338.3	18.362	39.80	420.3	14.88	0.54
IW-4	780A-1H-2, 57-67	12	3	2.12	11.87	24.8	27.17	339.3	19.270	38.59	419.4	15.06	0.63
IW-5	780A-1H-2, 129-139	10	3	2.84	11.74	26.0	27.56	351.8	16.051	38.05	427.7	15.07	0.59
IW-1	780B-1R-6, 1-6-116	41	2	8.61	19.09	33.2	33.49	517.6	1.275	26.93	462.8	13.70	7.59
IW-1	780C-1R-3, 140-150	53	3	4.45	8.93	35.0	34.43	534.0	1.797	28.58	463.7	10.19	8.14
IW-2	780C-5R-1, 48-58	32	2	33.53	12.49	23.0	26.09	270.8	45.833	43.52	389.1	13.68	0.47
IW-3	780C-15R-1, 38-48	48	5	129.93	12.38	25.1	28.06	315.2	35.636	45.03	422.7	15.49	1.31
IW-1	780D-1X-2, 96-106	50	1	2.51	9.52	30.8	31.96	484.6	1.766	27.31	469.3	11.27	4.76
IW-2	780D-1X-3, 68-78	44	1	2.73	11.86	25.0	27.55	364.7	15.778	33.11	433.6	12.51	0.27
IW-3	780D-2X-1, 40-50	35	2	2.95	12.35	22.7	25.96	284.4	33.791	44.33	392.0	12.53	1.13
IW-4	780D-6X-1, 68-78	25	3	21.13	12.42	22.8	26.59	285.3	40.655	44.27	398.8	12.96	1.36
^a BW-5	780D-7X-1, 0-1	18	<i>in situ</i>	27.41	12.60	22.2	25.82	234.1	62.872	46.84	377.3	12.35	0.46
IW-6	780D-7X-5, 135-150	58	5	34.83	11.72	25.8	27.71	369.5	9.139	36.37	427.1	12.81	5.68
^a BW-7	780D-8X-1, 0-1	2.6	<i>in situ</i>	32.41	8.42		16.97	249.5	2.553	23.05	166.6	7.61	7.43

^aBW = Barnes *in-situ* sample. BW-7 consisted of 2.6 mL taken from the partially flushed copper coil. The fully flushed steel coil was saved for shore-based gas analyses. Values absent from table were not determined.

were obtained between 35 and 126 mbsf because of poor recovery.

Interstitial waters were collected at Site 780 using the Barnes *in-situ* water sampler, as well as by squeezing of unconsolidated serpentine samples. Operation of the Barnes tool is detailed in the "Explanatory Notes" (this volume). Two samples were recovered with this tool, both from Hole 780D. The first sample consisted of 18 mL of undiluted interstitial water in the steel coil that was analyzed on board the ship, and about 12 mL in a 45-mL copper coil that was crimp-sealed for shore-based determination of gases and their isotopes. The temperature measured downhole in the serpentine while this sample was being collected did not stabilize. The second sample consisted of a total of only 23 mL and was accompanied by a valid temperature measurement of 3.5°C, 2.0°C above the ambient temperature of ocean bottomwater at Site 780. Because of the small volume of interstitial water recovered, the steel coil was saved for shore-based analysis, and 2.6 mL were crimped off in the 20-mL copper coil on recovery and analyzed on board the ship. The copper coil was initially filled with distilled water, which was only partially flushed by interstitial water during sampling because of the small volume recovered. The 2.6-mL sample proved to be highly anomalous, having much lower pH, alkalinity, ammonia, sulfate, sodium, potassium, salinity, and chlorinity, and higher calcium, and especially magnesium, than the other samples from Hole 780D (Table 8). Because this sample was recovered from the copper coil, in which it had presumably mixed heavily with distilled water, data from this sample are highly questionable and thus were not plotted in Figures 10, 11, and 12.

The compositions of surface seawater and of interstitial waters from Holes 780A, 780B, 780C, and 780D are plotted in Figures 10, 11, and 12. Interstitial waters from all four Sites on and near Conical Seamount are plotted in the "Sediment/Fluid Geochemistry" section, Site 781 (this volume).

As in the case of the hydrocarbon gases, the dissolved ions in the interstitial waters of unconsolidated serpentine at Site 780 (Table 8) show extremely large concentration gradients near the seafloor. The pH of these waters increases to 11.4 at 0.5 mbsf and to 12.0 at 1.5 mbsf in Hole 780A, and to 12.4 at 3.0 mbsf in Hole 780D (Fig. 10). The highest pH measured at the site was 12.6, for a water collected with the Barnes *in-situ* sampler from a depth of 27 mbsf in Hole 780D.

The highest pH for a squeezed sample was 12.4, at 21 mbsf in the same hole. These pH values are even higher than those at Site 779 and are undoubtedly higher than or comparable to the highest pH values ever measured in interstitial waters of marine sediments. Not all of the near-surface samples have such high values of pH, however; two samples from 4.5 mbsf in Hole 780C and 8.6 mbsf in Hole 780B have a pH of about 9. This indicates that these extremely high gradients are not ubiquitous at the site, but may be patchy in their distribution. After increasing abruptly to about 12.4 in the upper few meters of serpentine, the pH persists at this value to the greatest depth sampled, 130 mbsf in Hole 780C. The single exception is a sample from 35 mbsf in Hole 780D that has a pH of 11.7. This sample has anomalous concentrations of most species, as will be shown later in this section.

The alkalinity of the interstitial waters displays a similar pattern to that of pH, increasing rapidly in the surficial serpentine to high values that persist to the maximum depth sampled (Fig. 10). As in the case of pH, the steepest near-surface gradients are found in Hole 780A, where alkalinity increases eight-fold over the seawater value within the upper 2 m, and Hole 780D, where it increases 14-fold over the upper 3 m. The highest alkalinity measured, 62.9 meq/kg, is that of the *in-situ* sample with the highest pH, from 27 mbsf in Hole 780D. These alkalinities are much higher than those found at Sites 778 and 779. Once again, some near-surface values are much lower than others, indicating that the very high near-surface gradients are localized. The same three samples from the upper 9 m with a much lower pH than the others also have much lower alkalinities, even lower than in seawater, that range from 1.3 to 1.8 meq/kg. The deepest sample from Hole 780D (at 35 mbsf) has a lower alkalinity and pH than other samples from similar depths.

The profiles of ammonia concentration with depth at Site 780 (Fig. 10) are similar to those for pH and alkalinity. The highest concentration reached is 268 $\mu\text{mol/kg}$, which is higher than that at Sites 778 and 779 and about three times higher than values at similar depths at Site 779. Concentrations of silica are low, although not as low as those in the same depth interval at Site 779. Except for three samples from Hole 780D, all values are less than or equal to 35 $\mu\text{mol/kg}$.

The profiles of sulfate with depth are similar to those for pH, alkalinity, and ammonia. However, their most remark-

Table 8 (continued).

Magnesium (mmol/ kg)	Bromide (mmol/ kg)	Silica (μ mol/ kg)	Ammonia (μ mol/ kg)	Phosphate (μ mol/ kg)	Hydrogen Sulfide (μ mol/ kg)
52.89	0.85	5	<5		
0.008	0.64	20	119		
0.017	0.67	21	104		
0.003	0.64	12	171	0.71	
0.003	0.71	19	137		
0.011	0.64	19	118		
40.499	0.69	24	21	<0.10	
51.39	0.78	35	13	0.27	
0.004	0.56	34	237	0.71	
0.005	0.50	32	264	0.16	
25.422	0.65	<5	43	<0.10	
0.021	0.41	24	141	0.16	2000
0.002	0.48	62	205	0.27	<250
0.003	0.48	48	224	0.27	<250
0.002	0.46	89	268		
0.026	0.53	14	139	<0.10	<250
54.560	0.77	12	20		

able feature is the large increase in concentration relative to seawater shown by all but three of the samples, the same three from less than 9 mbsf that have lower pH, alkalinity, and ammonia than the others. As in the case of these other species, the increases in sulfate occur within 0.5 to 3 m of the seafloor, producing large gradients in the near-surface unconsolidated serpentinite. Except for the deepest sample from 35 mbsf in Hole 780D, the high sulfate concentration persists with depth at a value of 43 to 47 mmol/kg, fully two-thirds higher than the concentration in seawater. The sulfate concentration increases at Site 779 as well, between 100 and 160 mbsf, but this increase is relative to a decrease at shallower levels, so that none of the values exceed the concentration in seawater. The increases relative to seawater at Site 780 are highly unusual and require either a large source of sulfate or a large sink for H_2O .

High concentrations of H_2S were encountered at Site 780, in spite of the increase in dissolved sulfate (Table 7). As was the case for Site 779, there was no odor of H_2S in the interstitial water samples, presumably because of their high pH. The presence of H_2S was detected by the formation of a white to pale yellow to rusty orange to dark brown precipitate that formed in all of the samples from Site 780 when mercuric chloride was added. Only small amounts of precipitate formed in the uppermost samples from Holes 780B, 780C, and 780D, from 8.6, 4.5, and 2.5 mbsf, respectively. This precipitate was especially heavy and dark in the samples from 1.5 mbsf in Hole 780A, 34 mbsf in Hole 780C, and 2.73 mbsf in Hole 780D. The concentration of H_2S was measured colorimetrically in the latter sample and was found to be about 2 mmol/kg. Three deeper samples from Hole 780D were also analyzed and were found to contain less than 250 μ mol/kg.

The concentration of magnesium in the interstitial waters at Site 780 is extremely low, except for the three samples from the upper 9 m in Holes 780B, 780C, and 780D (Fig. 11). Most values were so low that they could not be determined by the titration method; all values less than 0.5 mmol/kg in Table 8 were determined by flame atomic absorption spectrometry (FAAS). Magnesium decreases with depth to very low concentrations at Sites 778 and 779 as well, but this decrease occurs over the much larger depth interval of about 100 m. In Hole 780A, magnesium decreases to 8 μ mol/kg within 0.5 m of the seafloor. It decreases almost as abruptly in Hole 780D, to 2 μ mol/kg at only 3 mbsf. The sample from

35 mbsf in Hole 780D that has anomalously low pH, alkalinity, ammonia, silica, and sulfate has the same low concentration of magnesium as the other samples from depths greater than 9 mbsf. Thus, these anomalous values cannot be attributed to contamination by seawater during drilling and recovery of the core, because such contamination would have raised the concentration of magnesium in the sample.

The concentration of dissolved calcium also decreases abruptly with depth at Site 780, to 0.44 mmol/kg at 0.5 mbsf in Hole 780A and to 0.27 mmol/kg at 3 mbsf in Hole 780D (Fig. 11). These calcium concentrations are sufficiently low to make one suspect the titration results. For this reason, all values for calcium in Table 8 of less than 1 mmol/kg were determined by FAAS. The latter results were found to agree within 0.5 mmol/kg with the titration results. The low concentrations of calcium persist with depth at Site 780, except for the single anomalous sample from 35 mbsf in Hole 780D, in which calcium values rebound to about one-half the value of seawater. Calcium also decreases with depth at Site 779, although not as abruptly or to such low levels. It reaches a minimum of 1.6 mmol/kg between 108 and 227 mbsf, then increases again to the bottom of Hole 779A, but never reaches or exceeds the concentration in seawater. At Site 778, calcium increases with depth and exceeds the seawater value at all depths.

The profile of the concentration of sodium with depth closely resembles that for calcium in both shape and direction of change (Fig. 11). The near-surface gradients again are very steep, giving a maximum depletion of 19%. The direction of change at Site 780 is the opposite of that at Sites 778 and 779, where sodium increases with depth by up to 24%. The contrast in direction of change among the sites is true for potassium as well: whereas potassium values decreased with depth by one-third at both Sites 778 and 779, they increase by more than 50% at Site 780 (Fig. 11). The near-surface gradients again are steep, especially for Hole 780A.

The profiles of concentration with depth for salinity, chlorinity, and bromide (Fig. 12) all resemble those of sodium and calcium (Fig. 11). The decreases relative to seawater are large and occur abruptly in the near-surface serpentinite material. Salinity decreases by as much as 26%, and chlorinity decreases by up to 57%. Chlorinity decreases by 28% at 0.5 mbsf in Hole 780A and by 38% at 1.5 mbsf. In Hole 780D, chlorinity and bromide each decrease by 48% and salinity by 25% at a depth of only 3 mbsf.

Interpretation of Results from Sites 778, 779, and 780

The interstitial waters collected from serpentinite-rich sediments and serpentinite flows at Sites 778, 779, and 780 on Conical Seamount are highly unusual compared with waters from more typical deep-sea sediments, such as those sampled just off the seamount at Site 781. These differences are illustrated in the "Sediment/Fluid Geochemistry" section (Site 781, this volume), where the interstitial water compositions from all four sites are plotted together (Figs. 8, 9, and 10).

The most remarkable feature of the interstitial waters from Conical Seamount is a decrease in chlorinity and salinity relative to the values in seawater and in most deep-sea interstitial waters. This decrease is much larger at the summit Site 780, but also occurs at the flank Sites 778 and 779. Equally remarkable is the extreme abruptness of this decrease with depth in the summit holes, especially 780A and 780D. The decrease in chlorinity and salinity is accompanied by other remarkable changes, leading to a pH as high as 12.6, alkalinity

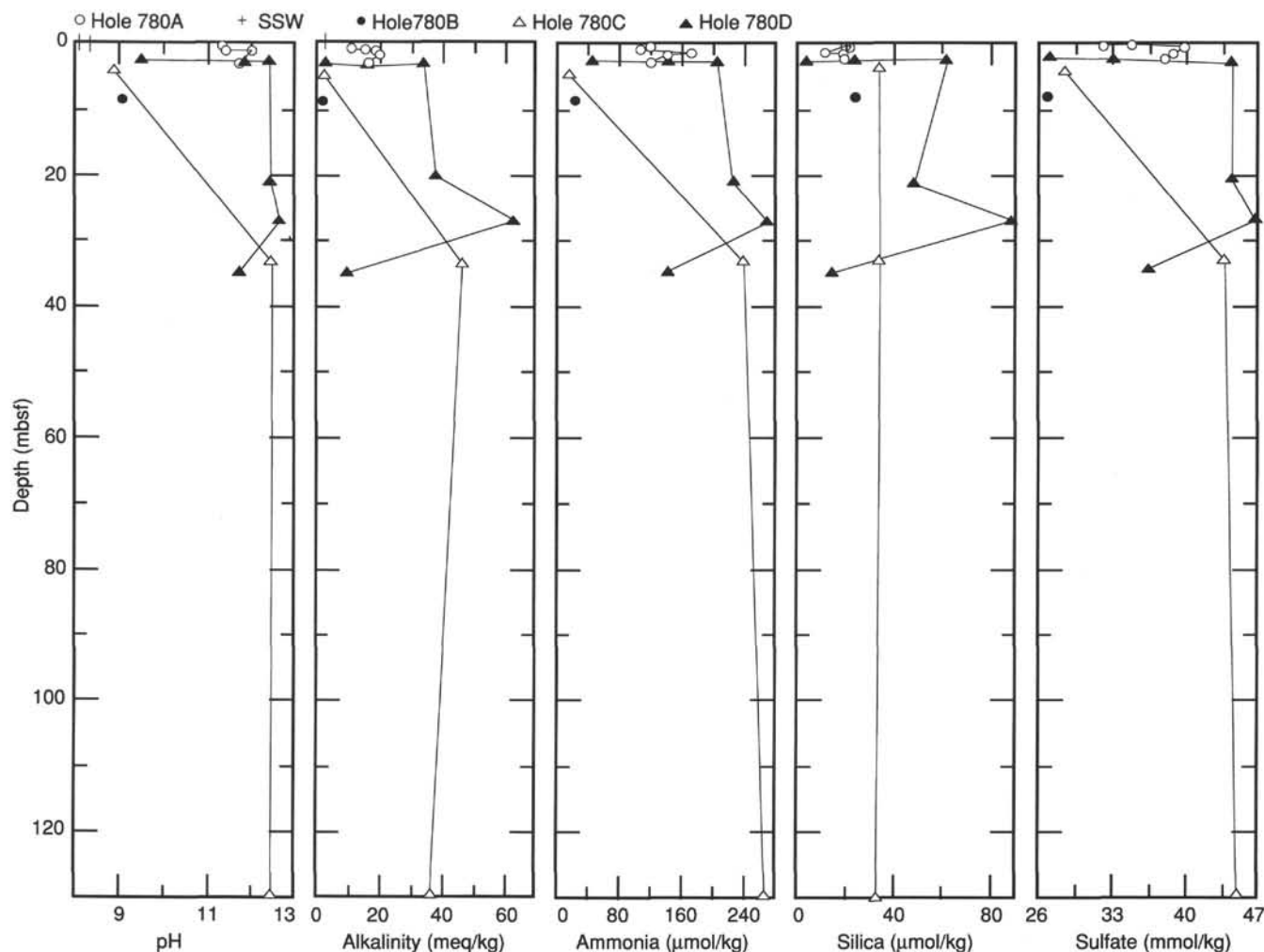


Figure 10. Composition of interstitial waters from cores at Site 780. SSW = surface seawater collected 22 February and 4 March 1989.

up to 26 times that of seawater, methane up to 38 mM, H_2S up to 2 mmol/kg, elevated ammonia, and very low concentrations of magnesium and silica. Sulfate, calcium, sodium, potassium, and alkalinity all change in one direction at the summit and in the other at one or both of the flank sites. Sulfate decreases with depth on the flanks, but increases by two-thirds at the summit. Calcium more than doubles at flank Site 778, but decreases at Site 779 and at the summit. Concentrations of sodium increase on the flanks, but decrease strongly at the summit, whereas potassium values decrease on the flanks and increase at the summit.

The central question regarding these interstitial waters is the cause of the decreases in chlorinity and salinity relative to seawater. Two possibilities exist: (1) the fluids originate mainly as seawater, and chloride is taken up by the solid phases during alteration in greater proportion than water; and (2) the fluids do not originate mainly as seawater, but contain a large component of less-saline water with a much lower chloride concentration than seawater. This less-saline water may have been produced by a number of processes, including membrane filtration through clays, decomposition of hydrocarbon gas hydrates, and dehydration of hydrous minerals.

Seawater-Rock Interaction and Chloride Uptake

Chloride uptake into solid phases during serpentinization has been reported, although the conditions under which this phenomenon can occur and the nature of the chlorine-rich phases are unclear. Janecky and Seyfried (1986) performed experiments reacting seawater and magnesium-free and magnesium- and sulfate-free seawater with peridotites at 200° and 300°C and a pressure of 500 bars. They found that dissolved chloride behaved conservatively when seawater was the reactant solution, but that significant chloride was taken up into partially serpentinized harzburgite when the starting solution lacked magnesium. The distinctive feature of the final solutions in the magnesium-free-seawater experiments was their high pH, which reached 11.5 in the longest experiment. This experiment was performed at a water/rock mass ratio of 10 and ran for 714 days. The loss of chloride from solution was 27 mmol/kg, indicating that the altered harzburgite must have contained about 10,000 ppm, or 1 wt%, chloride that it had picked up from solution during the experiment. Janecky and Seyfried (1986) were unable to determine in what solid phase or phases this chloride resided. They considered several possibilities: (1) a magnesium-iron-chloride mineral like iowaite, which has been reported from serpentinites

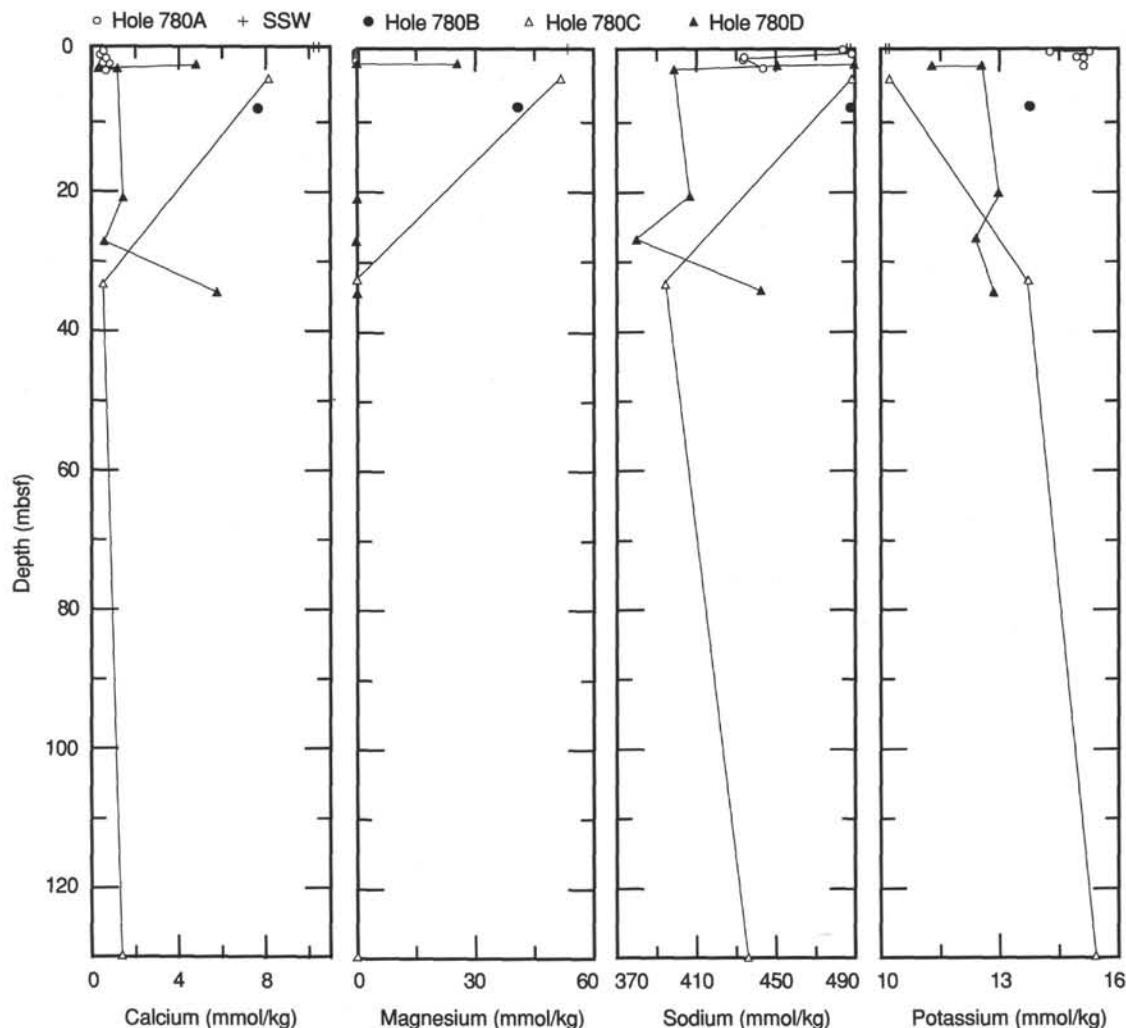


Figure 11. Composition of interstitial waters from cores at Site 780. SSW = surface seawater collected 22 February and 4 March 1989.

(Kohls and Rodda, 1967); (2) an iron-hydroxide-chloride phase, such as was suggested to occur in serpentinites by Rucklidge (1972) and Rucklidge and Patterson (1977); (3) a magnesium-hydroxide-chloride phase, $Mg_2(OH)_3Cl$, produced during experimental serpentinization at 500°C and 1000 bars by Poty et al. (1972); (4) newly formed, poorly crystallized serpentines that might retain chloride in their structure, as suggested by Miura et al. (1981); and (5) poorly crystallized brucite. Given that the chloride decrease in the longest experiment was balanced nearly mole for mole by a decrease in sodium, the latter two possibilities may be most likely. That this sodium did not appear in analyses of the altered rock from the experiment is puzzling and clouds any interpretation of the experimental data.

The large decreases in chlorinity in the interstitial waters at Site 780 are balanced only one-quarter to one-third by decreased sodium. When the nearly complete removal of magnesium and calcium from solution is included as well, only three-quarters of the charge loss can be accounted for. The other one-quarter is balanced about equally by the large gains in sulfate and alkalinity. Relative to seawater, the increase in sulfate is proportionally about equal to that in potassium. If the gains in sulfate and potassium are caused mainly by loss of water from seawater to the serpentinized rocks, and the rocks gain on average about 12 wt% water, then each gram of seawater would have reacted with and hydrated 2 to 3 g of fresh rock. If the rock also took up

chloride under these conditions, it would have to gain about 4300 ppm or 0.43 wt% chloride, to account for the chloride decrease observed in the interstitial waters at Site 780. This is well within the range of uptake that apparently occurred in the experiments of Janecky and Seyfried (1986).

There are two main problems with this hypothesis for the chlorinity decrease at Site 780. The first is that the concentration of bromide decreases along with chlorinity (Fig. 12). For most samples, the decrease in bromide is nearly, but not quite, as large as that of chlorinity. If the decrease in chlorinity is mainly the result of uptake of chloride into the altered rocks, then these rocks must be taking up bromide as well.

The second problem is that local reaction between rock and interstitial water probably cannot maintain the very large chemical gradients present in the upper few meters of serpentine sediment and flows at Site 780. To maintain these gradients, the process that lowers the chlorinity must be more rapid than diffusion of chloride from the overlying oceans into the interstitial waters of the near-surface serpentine materials. Otherwise, diffusion would lessen the gradients or erase them altogether. The near-surface lithology in which the gradients were measured consists mainly of the serpentine minerals; the only primary, unaltered phases that may be present are traces of opaque minerals and scattered amphibole. If these serpentine sediments and flows are capable of taking up chloride at

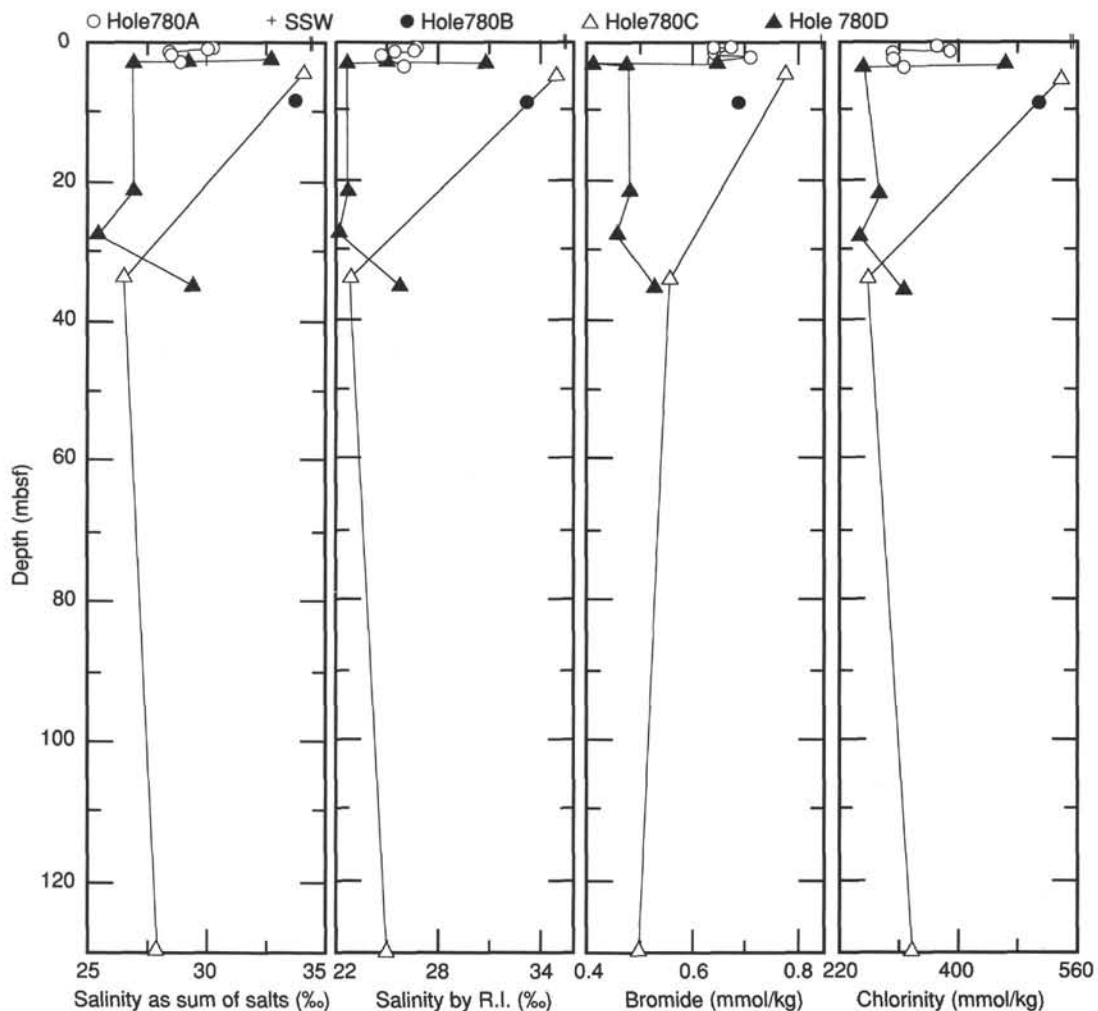


Figure 12. Composition of interstitial waters from cores at Site 780. SSW = surface seawater collected 22 February and 4 March 1989.

all, they should already have become saturated with it; it is highly unlikely that they are actively taking up chloride at the present time because they are already almost completely altered. If a water-rock reaction accompanied by chloride uptake is lowering the chlorinity of interstitial waters within Conical Seamount, this reaction must be occurring deeper in the system, below the maximum depth drilled. The less-saline water would then have to flow upward at Site 780 to maintain the high chlorinity gradients in the near-surface sediments.

The hypothesis of upflow at Site 780 is consistent with observations made from the manned submersible, *Alvin*, of chimneys constructed of calcite, aragonite, and poorly crystallized magnesium-silicates on the summit of Conical Seamount that were apparently precipitated from debouching fluids (Fryer et al., 1987; Haggerty, 1987c, 1989). The flow path and velocity of these solutions and the amount of fresh peridotite they may encounter on their way are not known at present. Whether the conditions encountered would allow uptake of sufficient chloride and bromide to produce the chloride-poor interstitial waters is also not known. However, one can be almost certain that these low-salinity interstitial waters do not originate by reaction within the depth range from which they were sampled, but have been transported there from elsewhere.

In addition to low chlorinity and salinity, the interstitial waters at Site 780 are characterized by high concentrations of methane, alkalinity, and ammonia. If our estimate of one-third to one-half for the seawater/rock mass ratio (based on the increases in sulfate and potassium) is accurate and relevant, then there would be adequate amounts of organic and carbonate carbon and nitrogen in the rocks (Table 5) to account for the observed concentrations of methane, alkalinity, and ammonia, respectively. Whether the rocks have actually supplied these species to the solutions is a question for further study. If the low-salinity fluids have in fact been transported into the sampled region from elsewhere, as concluded above, then the sampled unconsolidated serpentinite is not necessarily the source of these species.

Evidence from Drilling in Other Subduction Zones

Low-chlorinity interstitial waters have been sampled from drill holes in other subduction zones, including the Japan Trench, the Middle America Trench off Guatemala and Mexico, the Barbados accretionary prism, and the Peru continental margin.

In the Japan Trench, at Sites 438 and 439 drilled during Deep Sea Drilling Project (DSDP) Leg 57, the chlorinity of the interstitial waters decreases with depth to half the value in

seawater at 900 to 1100 mbsf. Moore and Gieskes (1980) suggested that this low-chlorinity water originated from a fossil aquifer.

In the Middle America Trench off Guatemala, the chlorinity of the interstitial waters is lower than that of seawater by up to 54% at 337 mbsf at Site 570 and at 395 mbsf at Site 497. Chlorinity also is lower by 6% to 41% at Sites 490, 491, and 492, drilled during DSDP Leg 66 off Mexico (Gieskes et al., 1985), Site 496, drilled during DSDP Leg 67 off Guatemala (Harrison et al., 1982), and Sites 565 and 568 drilled during DSDP Leg 84 off Guatemala (Hesse et al., 1985). The decrease in chlorinity at all these sites in the Middle America Trench has been attributed to the presence of hydrocarbon gas hydrates in the sediments. These hydrates decompose to methane and water during core recovery as a result of decompression and warming.

On the Northern Barbados Ridge, drilled during ODP Leg 110, chlorinity is lower than that in seawater by up to 28% at Site 674, but by less than 12% at all other sites drilled there. This decrease was tentatively attributed to an ultrafiltration process, in which clay minerals act as semipermeable membranes, selectively passing water but restricting the motions of ionic species (Shipboard Scientific Party, 1988a). Possible contributions from dehydration of smectites and melting of hydrocarbon gas hydrates were also considered. All of these processes were postulated to occur deeper than the maximum depth drilled; the freshwater produced is thought to move upward along faults and other permeable pathways, and especially along the shallowly inclined décollement surface.

On the Peru continental margin, chlorinity increases greatly with depth at five sites drilled during ODP Leg 112 and decreases at the other five. At Site 679, these decreases are up to 38% relative to seawater, but are less than 18% at the other four sites. Several processes may have contributed to these decreases in chlorinity, including decomposition of hydrocarbon gas hydrates, membrane filtration, dewatering of clays and opal, and the possible presence of fossil freshwater. Several chlorinity maxima and minima at Sites 682, 683, 685, and 688 clearly result from formation and decomposition, respectively, of gas hydrates at corresponding depths in the drill holes. As in the case of the Barbados accretionary prism, however, the larger scale decrease with depth suggests that the major source of freshwaters lies below the maximum depth drilled. These freshwaters are thought to have risen upward along permeable channels consisting of unconformities, coarse-grained sedimentary units, and conjugate and intersecting fracture zones (Shipboard Scientific Party, 1988b).

Possible Sources of Low-Chlorinity Water at the Conical Seamount Site

The 57% decrease in chlorinity at 27 mbsf in Hole 780D is larger than any observed in sediment interstitial waters above subduction zones elsewhere. It is also found at much shallower depths below the seafloor. As noted above, the strong chlorinity gradients within the upper few meters beneath the seafloor at Site 780 strongly suggest that interstitial water is flowing upward at this site.

The concentrations of methane at Site 780 may be high enough to stabilize methane hydrates under *in-situ* conditions, either within the sampled interval or at greater depths. These hydrates could supply freshwater on decomposition, either during core recovery if they lie within the sampled interval, or continuously if they are present at greater depths, at or near the bases of their stability fields. The profiles of chlorinity and methane with depth support the latter, deeper location rather than the former, as does the fact that no hydrocarbon gas

hydrates were recovered on Conical Seamount. On the other hand, we note that methane concentrations were up to 12 times higher at Site 779 than at Site 780, yet the chlorinity decrease at Site 779 was much smaller, only 9% lower than seawater, compared with 57% lower at Site 780. Unless methane and water derived from melting gas hydrates are somehow separated from each other within the upper few hundred meters of Conical Seamount, this discrepancy suggests that decomposition of gas hydrates is probably not the dominant source of freshwater on Conical Seamount.

Because of the low abundance of clay minerals in the rocks and sediments recovered from Conical Seamount, membrane filtration through clay minerals is an equally unlikely mechanism for generating freshwater. If this process is important, it would have to be taking place at greater depths than those drilled.

Dehydration of hydrous minerals at depth beneath Conical Seamount thus is the most likely mechanism for generating freshwater. The chemistry of the interstitial waters sampled at Sites 778, 779, and 780, especially the high pH, strongly suggests that the drilled interval is undergoing serpentinization at the present time. Thus, any dehydration of previously formed hydrous minerals would have to be taking place well below the maximum depth drilled.

Evidence for Mixing of Fluids from Several Sources

If the low-salinity fluids on Conical Seamount were not formed mainly by uptake of chloride into rocks during serpentinization, they must derive in part from some other, presumably deeper, source such as dewatering of the subducted lithospheric slab. From the composition of the interstitial waters at Site 780, we can infer that such waters should be rich in H₂O, CO₂, methane, ammonia, H₂S, and possibly also oxidized sulfur.

In addition to the general trends of an increase or decrease with depth relative to seawater, many of the dissolved species in the interstitial waters at Sites 778, 779, and 780 show more complex profiles that include maxima and minima. In particular, the lowermost one or two samples in Holes 778A, 779A, and 780D exhibit significant changes from the general trends. Interstitial waters from closely spaced holes at Sites 779 and 780 also show large differences in composition within a few meters beneath the seafloor.

Both types of variation might be caused by mixing of fluids of different composition from different sources in a complex plumbing system within Conical Seamount. At least two types of fluids are probably present in this setting: a low-salinity fluid that is ascending from depth, and locally derived seawater that has reacted with rocks and sediments in the vicinity of the seamount. We might also postulate that the latter fluid is of two types, one that has reacted mainly with mafic rocks and sediments and another that has reacted mainly with ultramafic rocks. The solutions ascending through the summit and exiting at Site 780 should be richer in the low-salinity fluid from depth, while the solutions sampled at the flank Sites 778 and 779 should be richer in the locally derived and reacted fluids. The deep fluid should have a high pH and be rich in methane, ethane, propane, alkalinity, ammonia, H₂S, sulfate, and potassium, and poor in silica, magnesium, calcium, chloride, and bromide. The fluid produced by local reaction of seawater with ultramafic rocks should have a high pH and be poor in silica and magnesium. The fluid produced by local reaction of seawater with mafic rocks and sediments should have a lower pH and be rich in silica, calcium, and sodium, and poor in alkalinity, sulfate, magnesium, and potassium. In this model, Site 778 should have the largest mafic-and-sediment component of the two flank sites, which would explain the relatively

low pH, alkalinity, and sulfate, and the higher concentrations of silica and calcium at this site. Site 779, with its complex profiles, especially of sulfate, calcium, and sodium, should exhibit the effects of mixing among all three fluids at various depths. A model with three separate fluids may be required to explain the maxima and minima in sulfate, calcium, and chlorinity in Hole 779A that generally do not correlate with one another. Additional modeling, including more chemical and mineralogical data for the solid phases, will be required to refine these interpretations.

STRUCTURAL STUDIES

Introduction

Structures in the materials recovered from Site 780 include (1) relict high-temperature, ductile to brittle fabrics in the un-serpentinized regions of ultramafic rocks; (2) symmetric and asymmetric serpentinization fabrics in some ultramafic rocks; (3) post-serpentinization deformation textures within serpentinite clasts; and (4) deformation within the serpentine matrix. In this section, we discuss these in turn and then briefly describe the results and structural implications of rheologic measurements of the serpentine matrix.

High-Temperature Structures in Unserpentinized Ultramafic Rocks

Relict minerals and textures are locally preserved in incompletely serpentinized rocks from Holes 780C and 780D. Some blocks are as little as 50% serpentinized, and the less-serpentinized areas of these blocks contain as little as 30% of serpentine minerals. High-temperature deformation fabrics that developed in the peridotite before serpentinization are preserved in these areas. The fabrics include undulatory extinction, common in both olivine and orthopyroxene, as well as some kink-banding of orthopyroxene and twinning of olivine. In Sample 125-780C-16R-1, 53–59 cm, some of the rock is essentially unstrained, while a shear band marked by necked and pulled-apart olivine can be observed only a centimeter away.

These textures are typical of mantle deformation. In some samples, deformation is distributed throughout the rock and probably occurred at relatively high temperatures and/or low strain rates. In others (e.g., Interval 125-780C-16R-1, 53–59 cm), the deformation is concentrated in relatively narrow shear bands; it is more brittle and appears to have taken place at relatively low temperatures and/or high strain rates.

Serpentinization Textures

Partly to completely serpentinized ultramafic blocks were recovered from both Holes 780C and 780D. Thin sections of these blocks reveal a wide range of textures that appear to reflect serpentinization under isotropic and anisotropic stress conditions, as well as in different temperature (and pressure?) regimes. Serpentinization fabrics observed in the rocks recovered from Holes 780C and 780D include mesh, felted-lath, and bladed-sheaf textures. In addition, late serpentine veins cross-cut previously formed serpentinization textures.

Mesh Textures

The cores of many incompletely serpentinized rocks exhibit anastomosing or weblike patterns of dark veins that separate islands of lighter gray rock. These webs of veins may exhibit a crude orthorhombic geometry, one of the ingredients of a "mesh" texture. Locally, bastite grains (serpentine pseudomorphs after orthopyroxene) straddle the boundary between dark veins and the adjoining lighter areas. Examination of these veins in thin section reveals that they are regions where the rock has been completely serpentinized, while the

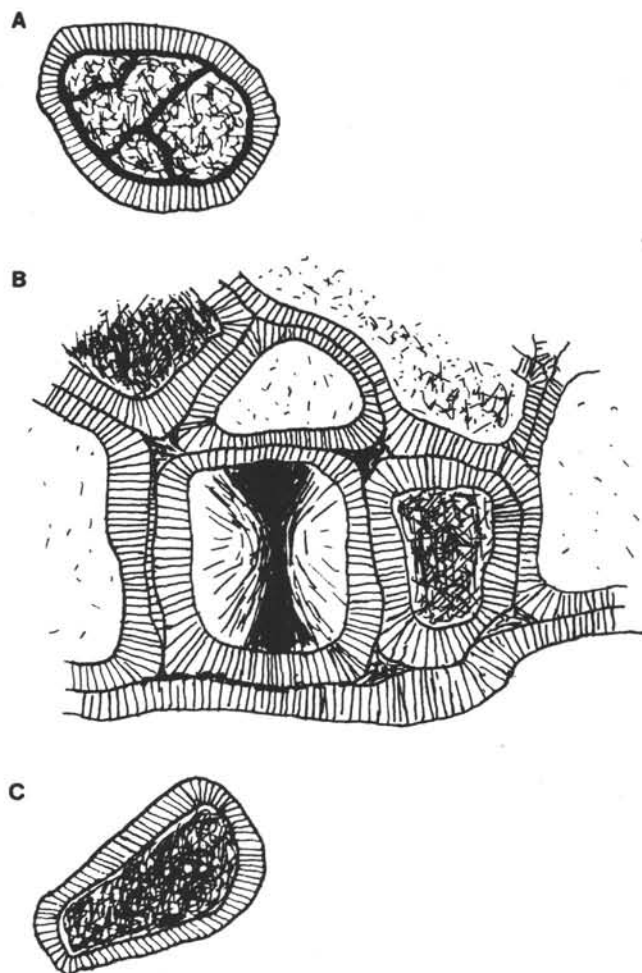


Figure 13. Representative serpentinization textures from mesh-texture serpentinites: A. Symmetric fibrous "halo" around relict olivine grain. B. Serpentine tablet with "hourglass" texture, surrounded by fiber halo. C. Asymmetric fiber halo.

adjoining gray areas preserve relict mineralogy. We refer to these veins as *serpentinization veins*. Serpentinization veins appear to bound many blocks.

In the less-serpentinized areas between the veins, orthopyroxene is commonly partially serpentinized along cleavage planes, and small olivine grains are separated by a mesh or web of serpentine veins (Fig. 13A). Groups of these small grains have parallel optical orientations, demonstrating that they are actually subgrain remnants of large olivine grains. A serpentine halo, typically consisting of fibrous serpentine minerals, surrounds each subgrain. These haloes adjoin and form the microscopic vein network. Where the haloes abut, a median line or zone is typically present; this may itself be filled with fibrous serpentine, or with magnetite grains. In some instances, stringers of opaque minerals (probably magnetite) line the centers of large veins of fibrous serpentine that surround relict subgrains with the same optical orientation. These magnetite stringers outline crude polygons.

In completely serpentinized rocks, and in serpentinization veins in incompletely serpentinized rocks, orthopyroxene has been completely altered to bastite, while relict olivine subgrains have been altered to tablets of serpentine, probably mostly lizardite. These tablets commonly exhibit "hourglass" texture, in which subgrains reach optical extinction in triangular quadrants with apexes at the center of the subgrains and

bases along their edges (Fig. 13B). Like their olivine-subgrain predecessors, these tablets are rimmed by haloes of fibrous serpentine. Opaque stringers similar to those in less-serpentinized areas are also common.

In many rocks (for example, Sample 125-780C-8R-1, 98–101 cm), the fibers in serpentine haloes extend radially outward from each relict olivine subgrain or serpentine tablet to the middle of the vein, and are symmetrical about the subgrain and perpendicular to its surface. In these rocks, the polygons outlined by the magnetite stringers are typically equant. In other rocks, however (for example, Sample 125-780D-7X-5, 94–96 cm), the fibers exhibit preferred orientation and are oblique to the olivine subgrain boundary and to the middle of the vein (Fig. 13C). In these rocks, the magnetite polygons may exhibit distinct elongation and preferred orientation.

Feltd-Lath Textures

Thin sections of two rocks (Samples 125-780C-10R-6, 36–37 cm, and 125-780D-2X-1, 7–8 cm) reveal “feltd-lath” textures, in which laths of serpentine minerals are feltd together to form a fine-grained, interlocking mass. Under crossed polarizers, this fabric appears to have a strong preferred orientation, with two sets of laths at approximately 90° to each other. However, the thin section looks the same in all orientations as the stage is rotated. In reality, the fabric is virtually isotropic, and displays only a weak preferred orientation.

Bladed-Sheaf Texture

In one thin section (Sample 125-780D-7X-1, 25–26 cm), antigorite is present as patches or sheaves of parallel blades. The blades within each patch have nearly the same optical orientation, but the rock is a mass of different patches, each with its own orientation. In the one example studied, this fabric does not appear to have a preferred orientation.

In most of the lizardite-chrysotile serpentinites recovered from Site 780, the serpentine fiber haloes that developed around olivine subgrains are symmetrical and isotropic, both in serpentinization veins and in less-serpentinized areas between the veins. Moreover, the magnetite polygons that presumably mimic the shapes of old olivine grains are not elongate and do not exhibit preferred orientation. These symmetrical textures probably indicate that the rocks were serpentinized under approximately isotropic stress conditions. Likewise, the feltd-lath and bladed-sheaf textures that developed in some of the rocks appear to be isotropic and probably also recrystallized under low deviatoric stresses. In one specimen (Sample 125-780D-7X-5, 94–96 cm), however, fiber haloes and magnetite polygons appear to have weak asymmetry, suggesting that this rock was recrystallized under anisotropic stress conditions.

In one of the samples exhibiting feltd-lath texture, (Sample 125-780D-2X-1, 7–8 cm), the fabric is developed in the serpentine matrix of a metaclastic rock that itself contains many detrital serpentine grains, in addition to rare brown hornblende, plagioclase, and carbonate clasts. The matrix of this detrital rock clearly recrystallized after its deposition.

Serpentine Veins

Many serpentinized ultramafic blocks from Site 780 contain veins of serpentine minerals that crosscut earlier serpentinization fabrics. Typically, these veins are filled with white to light green, fibrous serpentine that has grown perpendicular to the vein boundaries. We refer to these as *serpentine veins*. Many of these macroscopic fiber veins are found approximately in the centers of major, earlier serpentinization veins. In some cases, these cross-fiber veins have been intersected

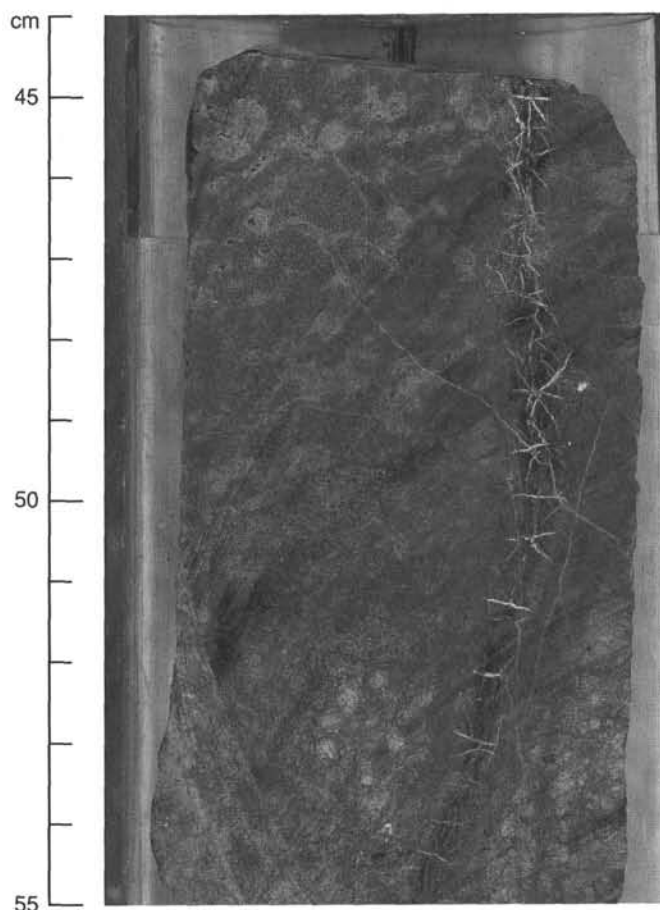


Figure 14. “Frankenstein” vein (serpentine veins cutting serpentinization vein) in Sample 125-780C-8R-1, 44–55 cm.

by a series of roughly perpendicular veins containing shorter fibers that extend across the serpentinization veins and, in some samples, a short distance into the surrounding rocks. We refer to this as “Frankenstein” texture; the main vein represents the incision and the cross-veins, the sutures. A good example is Sample 125-780C-8R-1, 44–55 cm, pictured in Figure 14.

The presence of serpentinization veins along block boundaries suggests that these veins are weak and have formed preferred zones of brittle failure along which large bodies of massive serpentinite fragment into smaller blocks.

The serpentine fiber veins in the samples are clearly extensional features in which new serpentine minerals have been deposited, rather than replacement veins. The common presence of these veins in the centers of earlier serpentinization veins is another indication that these serpentinization veins were zones of relative weakening and embrittlement of the rock. They also indicate that a common stress mechanism causes major serpentinization veins to fail in extension. The presence of “Frankenstein” veins indicates that the stress mechanism may be the expansion of the adjoining, less-serpentinized rock as it continues to serpentinize and expand. This expansion should exert tractions on the serpentinization vein, both along and across its length. Because the serpentinization vein cannot expand further, it experiences brittle failure in extension and the opening cracks fill with serpentine cross-fibers, resulting in the “Frankenstein” textures (Fig. 15).

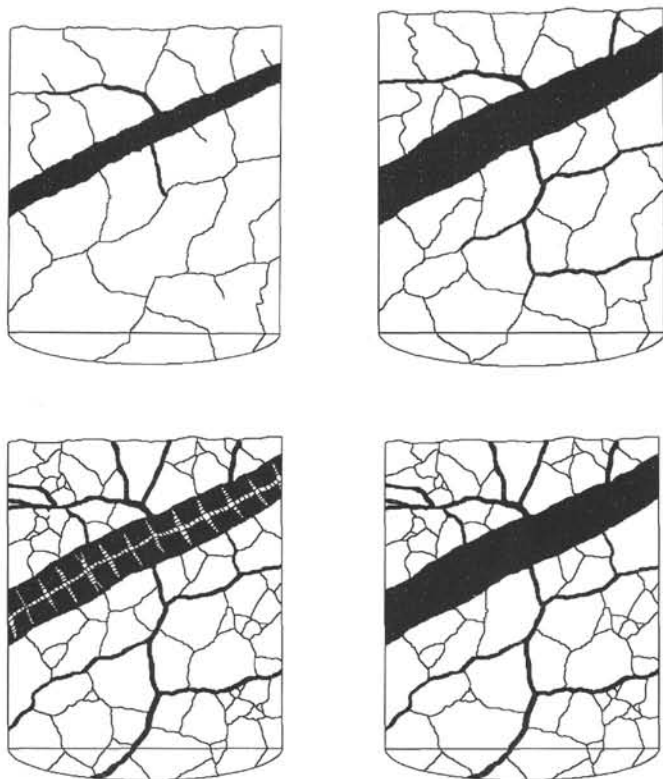


Figure 15. Stages in the growth of a "Frankenstein" vein.

Post-Serpentinization Deformation

Slight deformation after serpentinization is evinced by the kinking of fibers in veins and by irregular undulatory extinction in serpentine mesh structure. Typically, fibers appear to have been shortened parallel to their length, as well as to have undergone simple shear; oblique extensional fabrics (brittle "normal faults" or ductile shear bands) were not observed. Otherwise, little pattern is visible in these deformational features.

Deformation Textures in Serpentine Matrix

A striking feature of the serpentine matrix recovered from Site 780, especially in comparison with matrix from Sites 778 and 779, is the virtual absence of sheared foliation fabrics. In contrast, apparently detrital textures (clasts scattered in matrix and subhorizontal lamination) are common in the upper parts of the cores (Fig. 16). Matrix recovery was generally poor in the lower parts of the holes, but the approximately 3 m of matrix recovered from a depth of 30 m at the bottom of Hole 780D shows clast-in-matrix textures with no shear foliation; faint subhorizontal boundaries between muds of lightly different color can also be seen.

We interpret these undeformed fabrics as primary textures of the upwelling serpentinite and of the pools of serpentinitous material formed on top of the seamount. We think that the foliated, sheared, and convoluted fabrics at Sites 778 and 779 were superimposed on the structureless unconsolidated serpentine when it became unstable and began to flow down the slopes of the seamount.

Rheology of Serpentine Sediments and Flows

We conducted extensive tests of the stress-strain behavior of serpentine sediments and flows from Hole 780D using a Wykeham Farrance torsion-vane (torvane) apparatus. These

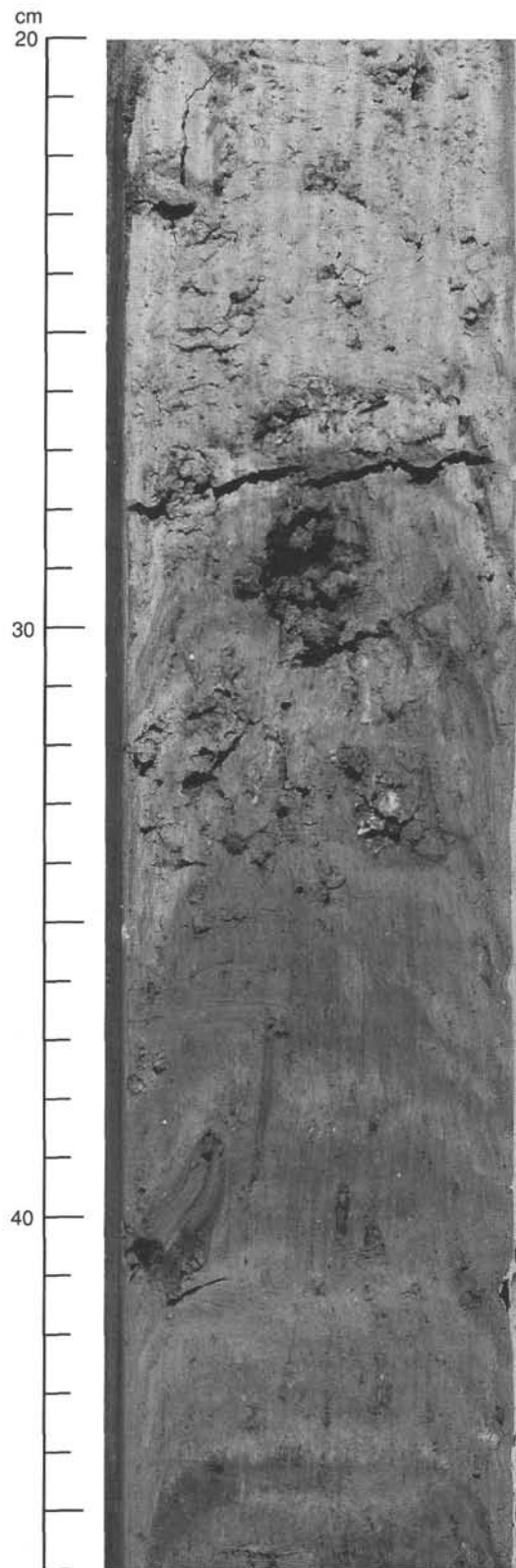


Figure 16. Clast-in-matrix textures and subhorizontal lamination in Sample 125-780D-1X-3, 20-46 cm.

Table 9. Ultimate strengths of serpentine sediments and flows recovered from Hole 780D.

Core, section, interval (cm)	Depth (mbsf)	Stress (kPa)
125-780D-1X-3, 48	1.91	14.5
125-780D-2X-2, 14	3.07	7.1
125-780D-2X-2, 27	3.07	7.3
125-780D-2X-CC, 16	3.87	16.4
125-780D-2X-CC, 23	3.89	18.1
125-780D-2X-CC, 31	3.90	20.1
125-780D-3X-1, 12	12.07	37.5
125-780D-6X-1, 71	21.00	9.1
125-780D-6X-2, 26	21.39	2.7
125-780D-6X-2, 41	21.52	5.2
125-780D-6X-2, 52	21.63	3.8
125-780D-6X-2, 65	21.64	4.0
125-780D-7X-1, 8	27.55	7.1
125-780D-7X-1, 30	27.63	7.5
125-780D-7X-1, 40	27.80	11.7
125-780D-7X-1, 46	27.86	26.9
125-780D-7X-1, 64	27.97	24.6
125-780D-7X-1, 73	28.01	18.6
125-780D-7X-1, 128	27.45	10.0
125-780D-7X-5, 51	28.52	3.0
125-780D-7X-5, 75	28.76	2.2
125-780D-7X-5, 125	29.27	1.3
125-780D-7X-6, 95	30.46	4.2
125-780D-7X-CC, 32	30.74	8.2

tests reveal that the serpentine materials are highly non-ideal and plastic, with ultimate strengths ranging from 1.3 to 38 kPa and averaging 11.6 kPa (see Table 9). For comparison, more "normal" oceanic muds recovered from Site 781 were somewhat stronger, having ultimate strengths ranging from 8.1 to 116.1 kPa. In only two cases did the samples actually fail; most serpentine merely continued to deform at a constant rate at maximum (ultimate) strength. Although we were unable to determine yield strength directly, our observations of the behavior of these materials as they were tested led us to think that their yield strengths are vanishingly low. Representative stress-strain curves for these materials are given in Figure 17.

These rheologic measurements suggest several important conclusions about the mechanics of the formation of Conical Seamount. First, modeling based on the ultimate strengths of the materials suggests that they might carry blocks of serpentinized peridotite (density approximately 2.6–2.7 g/cm³) as large as 20 m upward against the force of gravity. Second, their low yield strengths suggest that unless the material continues to well upward from within the feeder of the seamount, the blocks will fall back downward into the feeder. Finally, their low strengths suggest that the seamount is rheologically more like a mud volcano than a salt diapir (salt has an ultimate strength of approximately 10⁴ to 10⁵ kPa). This in turn suggests that the serpentine feeder may be relatively narrow with respect to the width of the edifice.

PALEOMAGNETISM

Magnetostratigraphy was impossible at Site 780 because of the lack of coherent lithologic units, the poor recovery, and the tectonized nature of the rocks. The natural remanent magnetization (NRM) of the archive half of each core was measured and demagnetized with the cryogenic magnetometer and the on-line AF demagnetizer at the 0-, 5-, and 10-mT levels. Several discrete samples (125-780C-1R-1, 95–97 cm; 125-780C-1R-2, 137–139 cm; 125-780C-1R-3, 95–97 cm; 125-780C-1R-4, 61–63 cm) were progressively demagnetized and measured at the 0-, 3-, 5-, 8-, 10-, 12-, and 15-mT levels.

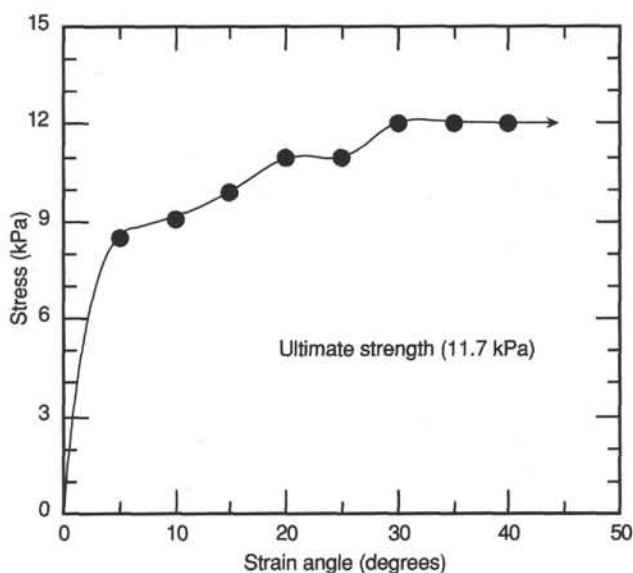


Figure 17. Representative stress-strain curves for serpentine matrix recovered from Hole 780D.

The rocks from Holes 780A, 780B, and 780D display scattered magnetic directions, making the determination of a magnetic polarity for any of the cores impossible. The magnetic intensities of these rocks vary between 10 and 1000 mA/m. In Hole 780C, the magnetic inclination in Core 125-780C-1R moved from steeply positive to predominantly negative at the 10-mT demagnetization level, suggesting a reversed polarity at the top of this hole (Figs. 18A and 18B). However, all of the discrete samples taken from Core 125-780C-1R show a positive inclination after demagnetization to 15 mT (Table 10). Contradictory data make it impossible to define a magnetostratigraphy for Core 125-780C-1R.

Magnetic susceptibilities were measured on the multisensor track. Many of the cores from Hole 780C were not measured because recovery was poor and the rocks in the cores were broken and disturbed by drilling. In Holes 780B, 780C, and 780D, the magnetic susceptibility ranged between $2\pi \times 10^{-3}$ to $10\pi \times 10^{-3}$ SI, with most of the measurements in the uppermost part of this range. In Hole 780A, Core 125-780A-1H shows a generally higher overall susceptibility than the rocks from the other holes in Site 780. The values in this core range from $8\pi \times 10^{-3}$ to $12\pi \times 10^{-3}$ SI. The magnetic susceptibility data display a regular scalloping pattern that has a wavelength of about 40 cm (Fig. 19), an interesting, but at this point inexplicable, observation. However, owing to the poor recovery and lack of coherent units, no systematic downhole changes in susceptibility were observed.

PHYSICAL PROPERTIES

Physical Properties Procedure

Physical and index properties measured at Site 780 are listed in Tables 11 and 12. Shear strength and sonic velocities were determined where possible. Some of the serpentine sediments and flows were too weak to measure shear strength accurately. Shear strengths were obtained for Hole 780D and are reported in the "Structural Studies" section (this chapter). Sonic velocities were determined using the Hamilton Frame apparatus on the hard clasts that were distributed through the serpentine material in Hole 780C. Velocities are reported in

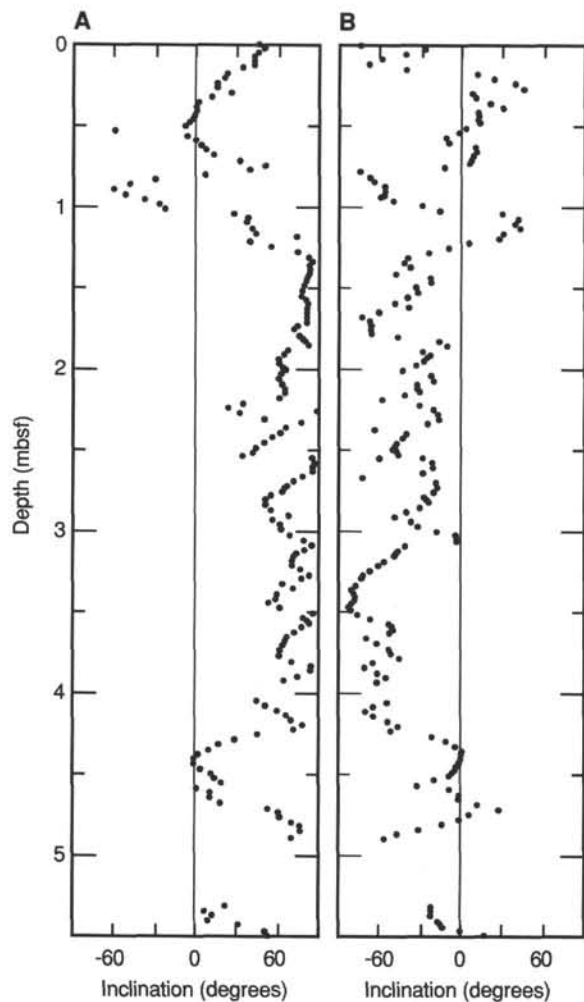


Figure 18. A. NRM inclination data (in degrees) from Core 125-780C-1R at 0 mT. B. Inclination data (in degrees) from Core 125-780C-1R after 10-mT demagnetization.

the "A" direction, parallel to the core axis, and in the "B" direction, normal to the core axis.

Hole 780A

Hole 780A was cored to only 3.5 mbsf. Table 11 lists the index properties, and Table 12 lists the thermal conductivities of material from this core. The average bulk density is 1.83 g/cm³, and the average grain density is 2.64 g/cm³. The GRAPE provided accurate values of bulk density in this hole (Fig. 20). The high bulk-density value of these sediments reflects the density of serpentine, 2.5 to 2.65 g/cm³, and the water content, about 30%.

Hole 780B

Hole 780B was cored to 18.2 mbsf, with 0.34 m recovered. Table 11 lists the index properties, and Table 12 presents thermal conductivities of material from this core. The average bulk density is 1.73 g/cm³, and average grain density is 2.63 g/cm³.

Hole 780C

Hole 780C, cored to 163.5 mbsf, is the deepest hole at this site. The poor recovery (only 8.8%), probably caused by alteration of weak serpentine sediments and flows and clasts of hard rock, leaves large gaps in the record of physical

Table 10. Paleomagnetic data for discrete specimens taken from Core 125-780C-1R.

Section, interval (cm)	Natural remanent magnetization			Polarity
	Declination (degrees)	Inclination (degrees)	Intensity (mA/m)	
IR-1, 95	352.7	-12.1	356.0	
IR-2, 137	171.1	84.5	83.0	
IR-3, 95	326.8	-25.2	230.0	
IR-4, 61	251.1	70.6	69.0	
IR-CC, 11	303.5	89.7	71.7	
Remanent magnetization after demagnetization to 15 mT				
IR-1, 95	74.6	56.1	6.04	N
IR-2, 137	122.2	60.1	4.18	N
IR-3, 95	235.8	76.8	6.06	N
IR-4, 61	175.3	50.6	3.52	N
IR-CC, 11	184.3	26.2	4.37	N

Note the large decrease in intensity for all specimens. The median destructive field value for these specimens averages less than 2 mT.

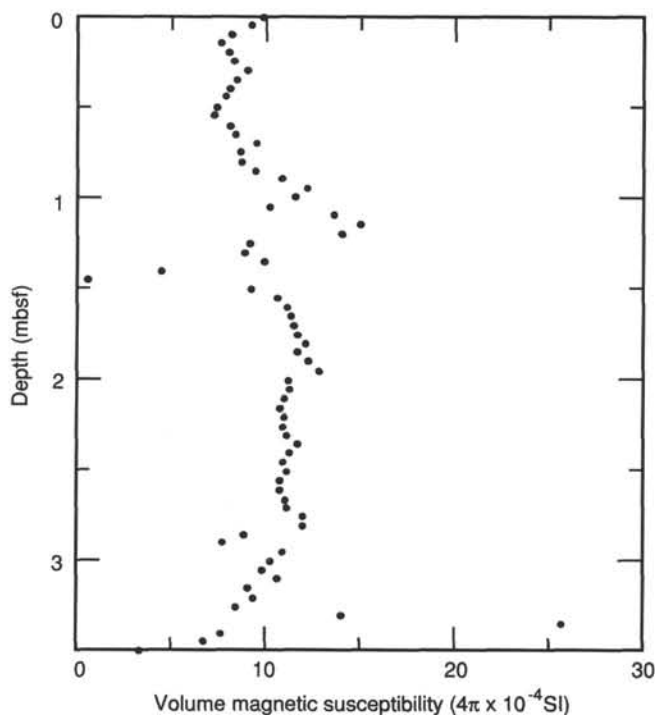


Figure 19. Volume magnetic susceptibility for upper portion of Core 125-780C-1R. Notice the scallop pattern, which has a wavelength of about 40 cm.

properties of materials from this hole. Tables 11 and 12 list the index properties, thermal conductivities, and sonic velocities of materials from this hole.

Figures 21 and 22 illustrate the index properties of materials from Hole 780C. The average bulk density of the matrix material is 1.77 g/cm³, and the average grain density is 2.65 g/cm³. The average bulk density of the clasts is 2.76 g/cm³, and the average grain density is 2.77 g/cm³. From Figures 21 through 22, one can see that no significant correlation exists between the index properties and depth. The distinction between the matrix and the clasts is clearly seen in Figures 21 and 22.

Figure 23 illustrates the variation of thermal conductivity with depth and shows no significant pattern. However, the thermal conductivity of the clasts is uniformly greater than that of the matrix material.

Table 11. Index properties for Holes 780A, 780B, 780C, and 780D.

Core-section, interval (cm)	Depth (mbsf)	Bulk density (g/cm ³)	Grain density (g/cm ³)	Porosity (%)	Water content (%)	Void ratio
125-780A-1H-1, 39-41	0.39	1.79	2.64	52.6	31.3	0.53
1H-1, 58-60	0.58	1.80	2.56	49.5	29.3	0.49
1H-2, 68-70	2.18	1.91	2.74	48.5	27.1	0.48
1H-CC, 23-25	3.13	1.82	2.63	50.6	29.60	0.51
125-780B-1R-1, 99-101	0.99	1.72	2.63	57.2	35.4	0.57
1R-2, 39-41	1.89	1.75	2.67	55.9	33.8	0.56
1R-3, 30-31	3.30	1.70	2.68	59.3	37.0	0.59
1R-4, 49-50	4.99	1.75	2.56	53.0	32.1	0.53
1R-6, 99-100	8.49	1.75	2.63	55.4	33.7	0.55
125-780C-1R-1, 72-74	0.72	1.64	2.68	62.86	40.61	0.63
1R-2, 64-66	1.68	1.63	2.64	62.72	40.81	0.63
1R-3, 89-91	3.43	1.65	2.57	59.63	38.34	0.60
1R-4, 76-78	4.80	1.71	2.69	58.75	36.41	0.59
2R-1, 30-32	5.80	1.71	2.63	57.36	35.58	0.57
3R-1, 56-59	14.56	3.06	3.06	00.18	00.06	0.00
4R-1, 13-15	23.63	1.75	2.62	54.60	33.11	0.55
5R-1, 41-43	33.41	1.83	2.66	51.14	29.76	0.51
6R-1, 61-62	43.11	2.70	2.70	00.07	00.03	0.00
7R-1, 13-15	52.20	2.05	2.66	37.58	19.49	0.38
8R-1, 98-101	62.48	2.67	2.67	00.18	00.07	0.00
9R-1, 34-37	71.44	2.78	2.80	00.95	00.36	0.01
10R-1, 13-16	80.93	2.74	2.75	00.42	00.16	0.00
12R-1, 17-20	100.37	2.64	2.65	00.59	00.24	0.01
13R-1, 40-43	106.90	2.92	2.92	00.11	00.04	0.00
15R-1, 23-25	125.73	1.81	2.64	51.85	30.48	0.62
15R-CC, 13-14	126.08	1.96	2.67	43.48	23.62	0.43
16R-1, 53-59	135.53	2.66	2.68	01.27	00.51	0.01
18R-1, 107-111	155.07	2.71	2.72	00.53	00.21	0.01
125-780D-1X-1, 20-22	0.20	1.65	2.75	63.8	41.0	0.64
1X-2, 52-54	0.97	1.69	2.58	57.7	36.4	0.58
1X-3, 45-47	1.96	1.83	2.72	53.1	30.9	0.53
1X-CC, 11-13	2.40	1.69	2.65	59.5	37.5	0.59
2X-1, 30-32	2.80	1.85	2.62	48.7	28.0	0.49
2X-2, 3-5	3.03	1.67	2.79	64.0	40.8	0.64
2X-CC, 4-6	3.82	1.71	2.68	58.8	36.6	0.59
3X-1, 13-15	12.13	1.47	2.11	60.2	43.7	0.60
5X-1, 9-11	16.99	2.55	2.57	1.1	0.5	0.01
6X-1, 62-64	21.02	1.67	2.64	60.4	38.5	0.60
6X-2, 41-43	21.59	1.64	2.88	66.7	43.1	0.67
7X-1, 43-45	27.83	1.95	2.83	48.7	26.5	0.49
7X-5, 45-47	28.53	1.68	2.66	60.4	38.3	0.60
7X-6, 13-15	29.71	1.69	2.67	59.7	37.4	0.60
7X-CC, 20-22	30.69	1.72	3.08	66.1	40.8	0.66

Figure 24 is a plot of the "A" and "B" velocities vs. depth. These velocities fall between 5000 and 6000 m/s and exhibit no correlation with depth.

Hole 780D

Hole 780D was cored to a depth of 32.4 mbsf, with 9.09 m recovered. Tables 11 and 12 list the index properties and thermal conductivities of the material from this core. The average bulk density is 1.71 g/cm³, and the average grain density is 2.66 g/cm³. Figures 25 and 26 present plots of bulk and grain densities vs. depth. With the exception of a few points, these properties do not vary systematically with depth. Figure 27 is a plot of thermal conductivity vs. depth and indicates a large amount of scatter.

LOGGING

Downhole temperatures were measured and logging was conducted at Site 780. We attempted to log Hole 780C and downhole temperatures were measured at Hole 780D using the Barnes-Uyeda tool. The logging data have been converted from mbrf (meters below rig floor) to mbsf. The Kelly bushing on the ship's rig floor was the reference point at 10.6 m above sea level, while the mud line is located 3083.4 mbsl (meters below sea level).

Logging

We decided to try to log Hole 780C, despite its shallow depth and drilling problems, because of the high scientific interest in this hole and the poor core recovery. The poor hole conditions were revealed when several large overpulls were necessary while the hole was being conditioned for logging, including a 300,000-lb overpull at 234 mbsf. At that same depth, a 260,000-lb overpull was necessary after the bit was dropped at the bottom of the hole.

Once the bit had been dropped, we set the end of the pipe at 56 mbsf. The first logging string consisted of the following tools (listed from the bottom of the string upward): the Lamont-Doherty temperature logging tool (TLT), the Schlumberger phasor induction tool (DIT), the Schlumberger litho-density tool (HLDT), and the Schlumberger sonic tool (SOT) (see the "Explanatory Notes," this volume, for more details of the tools). The tool string was run down to about 14 mbsf and held there. This served as a reference point for the TLT and allowed us to check the performance of the Schlumberger tools. We resumed lowering after 10 min and proceeded until the tool string touched down at 58 mbsf, just beyond the end of the drill string. The only tool that was outside the drill string at that point was the TLT. Various attempts were made to

Table 12. Physical properties for Holes 780A, 780B, 780C, and 780D.

Core-section, interval (cm)	Depth (mbsf)	Thermal conductivity (W/mK)	Resistivity (ohms)	Formation factor	"A" velocity (km/s)	"B" velocity (km/s)	Ultimate stress (kPa)
125-780A-1H-1, 13-5	0.07		48.0	5.60			
1H-1, 25-25	0.25	1.683					
1H-1, 71-75	0.73		72.0	8.40			
1H-1, 113-117	1.15		53.0	6.19			
1H-2, 25-25	1.75	1.791					
1H-CC, 23-25	3.13	1.901					
125-780B-1R-1, 54-54	0.54	1.161					
1R-2, 39-41	1.89	1.468					
1R-3, 73-73	3.73	1.342					
1R-4, 78-78	5.28	1.579					
1R-6, 41-41	7.91	1.352					
125-780C-1R-1, 72-74	0.72	0.821	22.0	2.57			
1R-2, 36-40	1.68		21.8	2.54			
1R-2, 64-66	1.88	1.434					
1R-2, 103-107	2.55		13.0	1.52			
1R-3, 89-91	3.43	1.254					
1R-3, 127-131	4.29		24.9	2.91			
1R-4, 106-108	5.10	1.350					
2R-1, 19-21	5.69	1.510					
3R-1, 21-33	14.21	2.271					
3R-1, 56-59	14.56				4.25	5.05	
4R-1, 13-15	23.63	1.411					
6R-1, 61-62	43.11	2.273			5.79	5.51	
8R-1, 98-101	62.48	2.648			5.65	5.82	
9R-1, 34-37	71.44	2.626			5.71	5.56	
10R-1, 13-16	80.93				5.18	5.43	
12R-1, 17-20	100.37	2.945			5.26	5.26	
13R-1, 40-43	106.90	3.457			6.21	6.19	
15R-1, 23-25	125.73	1.481					
16R-1, 53-59	135.53	2.293			5.3	5.54	
18R-1, 107-111	155.07	2.624			5.66	5.56	
125-780D-1X-1, 20-22	0.20	1.224					
1X-2, 26-26	0.71	1.244					
1X-3, 26-26	1.77	1.294					
1X-3, 48-48	1.91						14.5
1X-CC, 11-13	2.40	1.372					
2X-1, 30-32	2.80	1.270					
2X-2, 3-5	3.03	1.418					
2X-2, 14-14	3.07						7.1
2X-2, 27-27	3.20						7.3
2X-CC, 4-6	3.82	1.442					
2X-CC, 16-16	3.87						16.4
2X-CC, 23-23	3.94						18.1
2X-CC, 31-31	4.02						20.1
3X-1, 13-15	12.13	1.474					37.5
5X-1, 9-11	16.99	1.911					
6X-1, 44-46	20.84	1.201					
6X-1, 71-71	21.00						9.1
6X-2, 21-23	21.39	0.670					2.7
6X-2, 41-41	21.52						5.2
6X-2, 52-52	21.63						3.8
6X-2, 65-65	21.64						4.0
7X-1, 8-8							7.1
7X-1, 19-23	27.61	38.1		4.45			7.5
7X-1, 43-45	27.83	1.536					11.7
7X-1, 46-46							26.9
7X-1, 50-54	27.92		61.0	7.12			61.0
7X-1, 73-73	28.01						18.6
7X-1, 128-128	28.25						10.0
7X-5, 45-47	28.53	1.092					3.0
7X-5, 75-75	28.76						2.2
7X-5, 125-125	29.27						1.3
7X-6, 77-79	30.35	0.428					
7X-6, 95-95	30.46						4.2
7X-CC, 20-22	30.69	1.139					
7X-CC, 32-32	30.74						8.2

punch the tool through the hole obstruction by raising the tool string, then lowering it quickly, and by moving the drill string. We were unable to push through the obstruction even after trying for 1 hr and therefore decided to retrieve the tools. We felt that the hole had collapsed below the drill string and that attempts to clear it would not be successful, so we terminated the logging run.

The only useful data from this logging run were from the TLT. Quite unexpectedly, the temperature increased dramatically from a seafloor value of 1.52 to 13.5°C by 58 mbsf. Data from the fast-response thermistor are shown in Figure 28, and data from the more accurate slow-response thermistor are shown in Figure 29. Individual data points have been plotted together in Figure 30 for comparison. The differences between

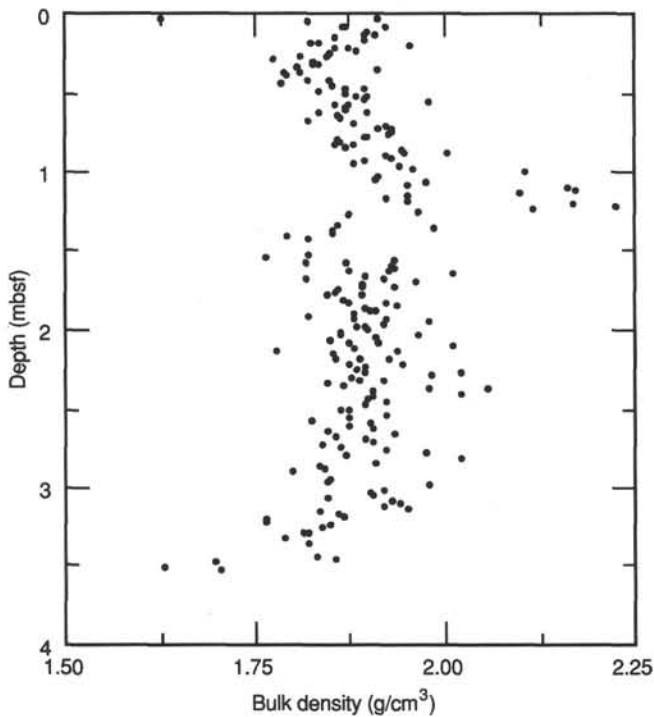


Figure 20. GRAPE-determined bulk density for Hole 780A.

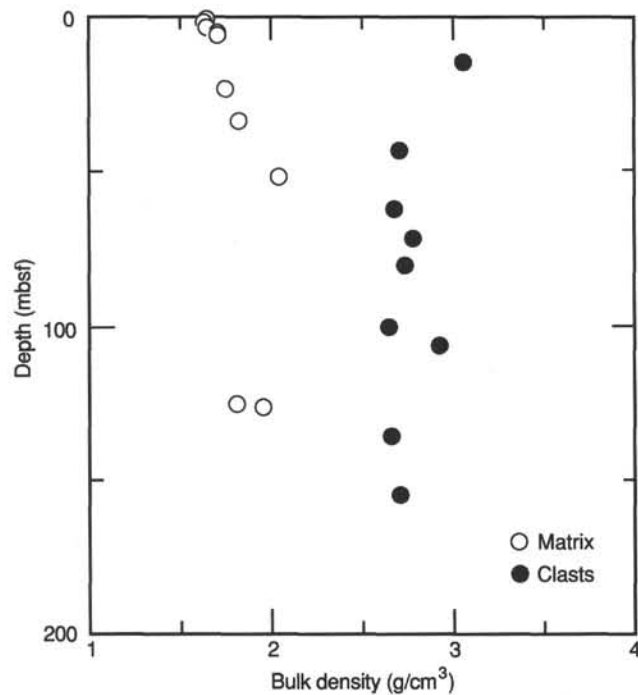


Figure 21. Depth vs. bulk density for Hole 780C. Data plotted as solid circles derive from clasts, and those plotted as open circles derive from the matrix.

the fast- and slow-response thermistors later in the record result from a coating of mud on the slow-response thermistor. A plot of the data over a shorter time interval is shown in Figure 31. The temperature starts to rise at about 1530 s, as the tool travels below the seafloor. Temperatures then increase at a fairly constant rate until about 1580 s, when temperatures again increase at a much faster rate until the

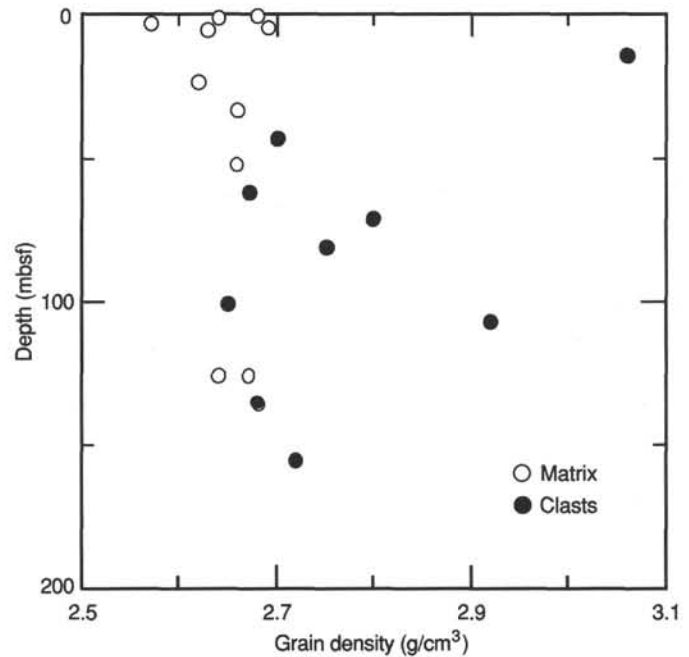


Figure 22. Depth vs. grain density for Hole 780C. Data plotted as solid circles derive from clasts, and those plotted as open circles derive from the matrix.

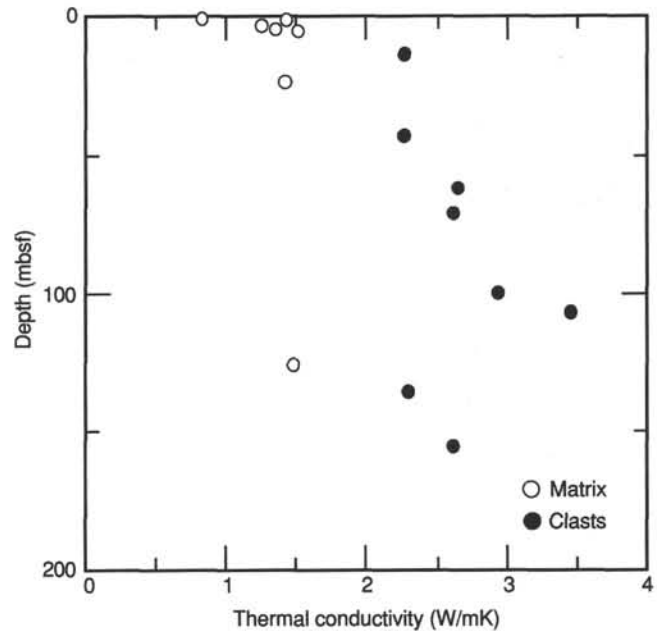


Figure 23. Depth vs. thermal conductivity for Hole 780C. Data plotted as solid circles derive from clasts, and those plotted as open circles derive from the matrix.

peak temperature is reached at about 1630 s. The reason for the change in the rate of the increase in temperature is not readily apparent. The TLT also has a pressure sensor, enabling us determine its depth in the hole. Pressure data are plotted vs. time in Figure 32. There is a large amount of short-term variability in these data because they represent information gained from lowering the logging string, when the wireline heave compensator is not in use. A smoothed version of these pressure data is shown in Figure 33. One can see that although there is a slight change in the rate of descent of the

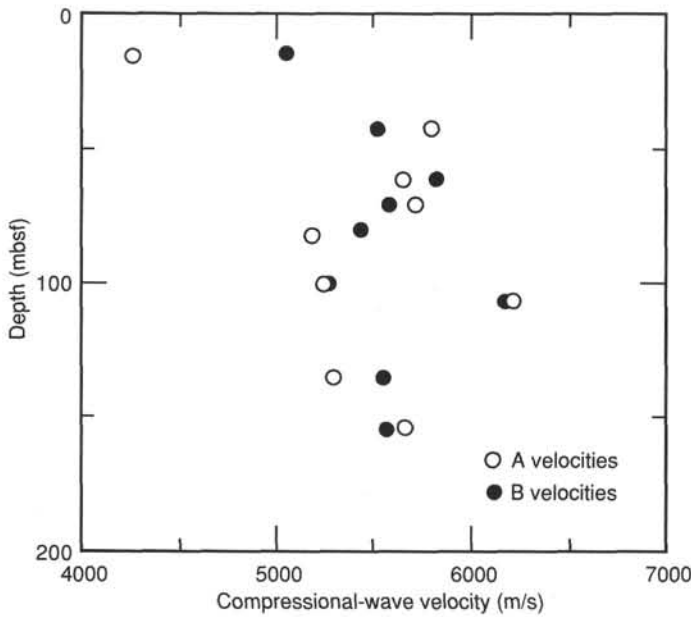


Figure 24. Depth vs. compressional-wave velocity for Hole 780C. Data plotted as solid circles represent *B* velocities, perpendicular to the core hole, and those plotted as open circles represent *A* velocities, parallel to the core hole.

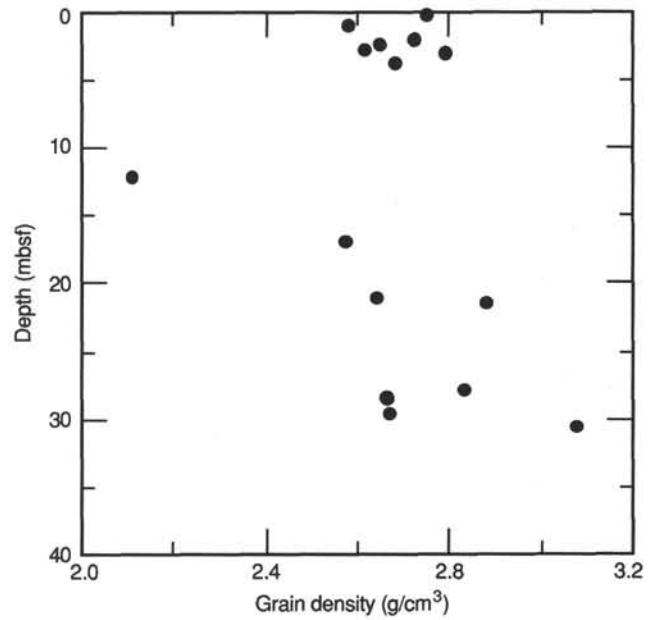


Figure 26. Depth vs. grain density for Hole 780D.

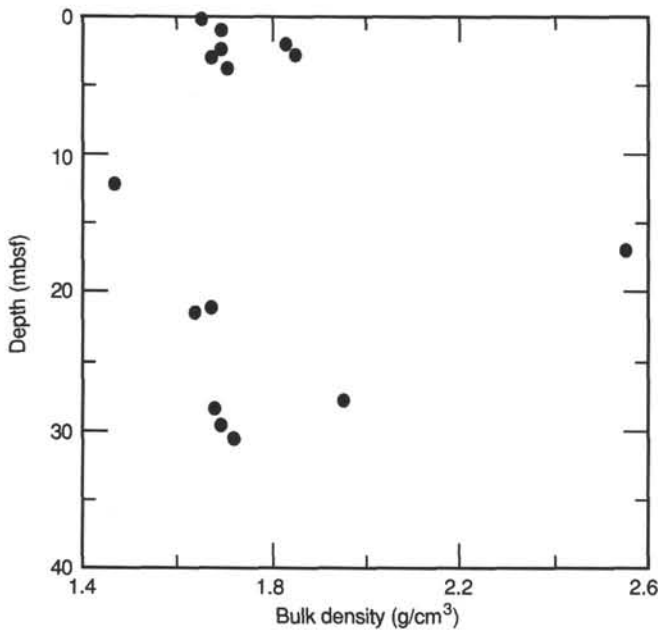


Figure 25. Depth vs. bulk density for Hole 780D.

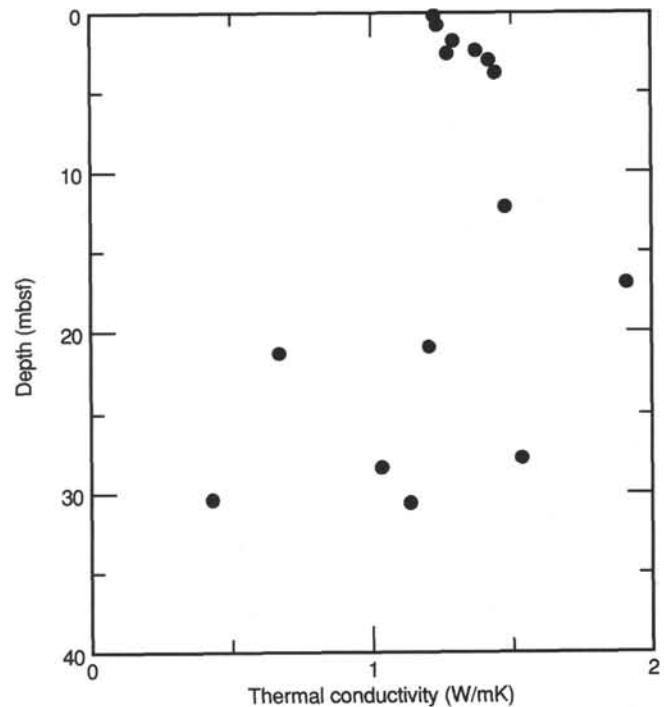


Figure 27. Depth vs. thermal conductivity for Hole 780D.

tool as it is being run into the drill pipe, it is not so dramatic a change as that of the temperature. Interpretation of these temperature results is discussed further below in comparison with results from the Barnes-Uyeda temperature tool.

Temperature Tool

The Barnes-Uyeda water sampler and temperature tool was used for three measurements in Hole 780D. Two temperature measurements were obtained, one during Run 06X at 20.4 mbsf and another during Run 08X at 41.8 mbsf. The temperature record from Run 06X is shown in Figure 34. This temperature record is somewhat noisy. The tool was seated at

about 59 min into the run, and there is a usable decay curve from then until about 75 min. A simplified correction for the decay of the frictional heating from emplacement is shown in Figure 35. After the first few minutes of emplacement, the decay curve is proportional to $1/\text{time}$. A linear least-squares regression on the data, extrapolated to $1/\text{time} = 0$, is a good estimate of the equilibrium sediment temperature. Run 06X gave an estimated temperature of 2.41°C, with an r^2 value of 0.975. This temperature value might be somewhat high, given the extra frictional heating that occurred before the probe was firmly seated in the bottom of the hole (Fig. 34). The temper-

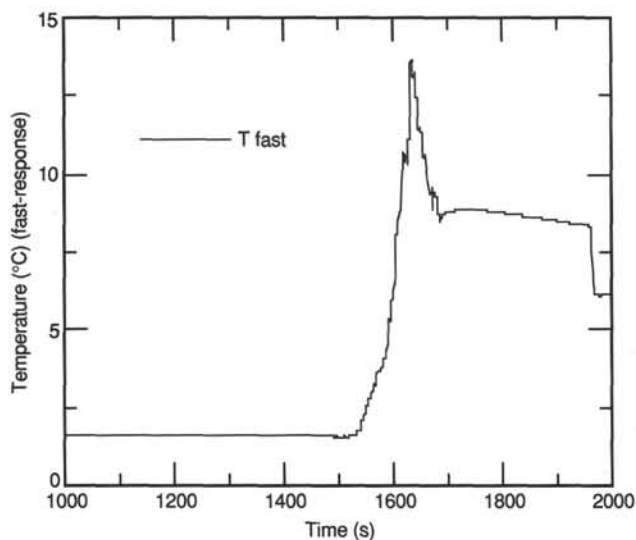


Figure 28. Temperature ($^{\circ}\text{C}$) measured with the fast-response thermistor of the temperature logging tool (TLT) vs. time.

ature record from Run 08X is shown in Figure 36. This decay curve is much cleaner for this run from the time the probe was seated in the bottom at 63 min, until pullout at 80 min. The corresponding equilibrium reduction plot, Figure 37, shows a much better fit than the one for Run 06X. The estimated equilibrium temperature is 3.10°C , with an r^2 value of 0.998.

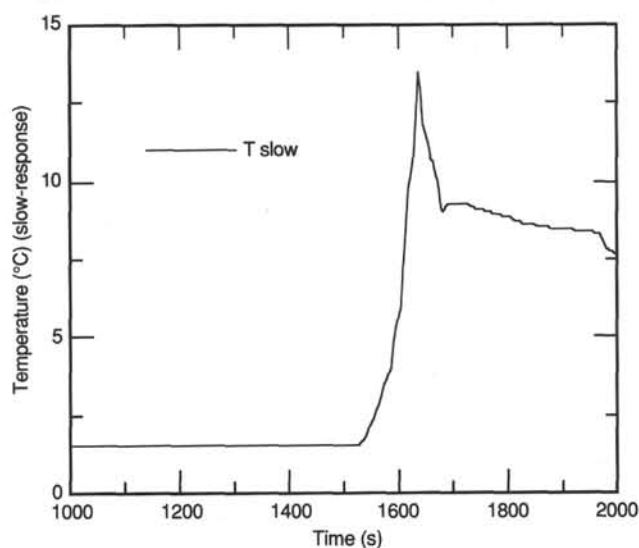


Figure 29. A plot similar to that in Figure 28, using the more precise slow-response thermistor.

The temperature data must be combined with the thermal conductivity data to determine the heat flow at this site. The thermal conductivity data are discussed in the "Physical Properties" section (this chapter). We combined all the thermal conductivity data for Site 780 (Holes 780A through 780D) in Figure 38. The most useful way to analyze the

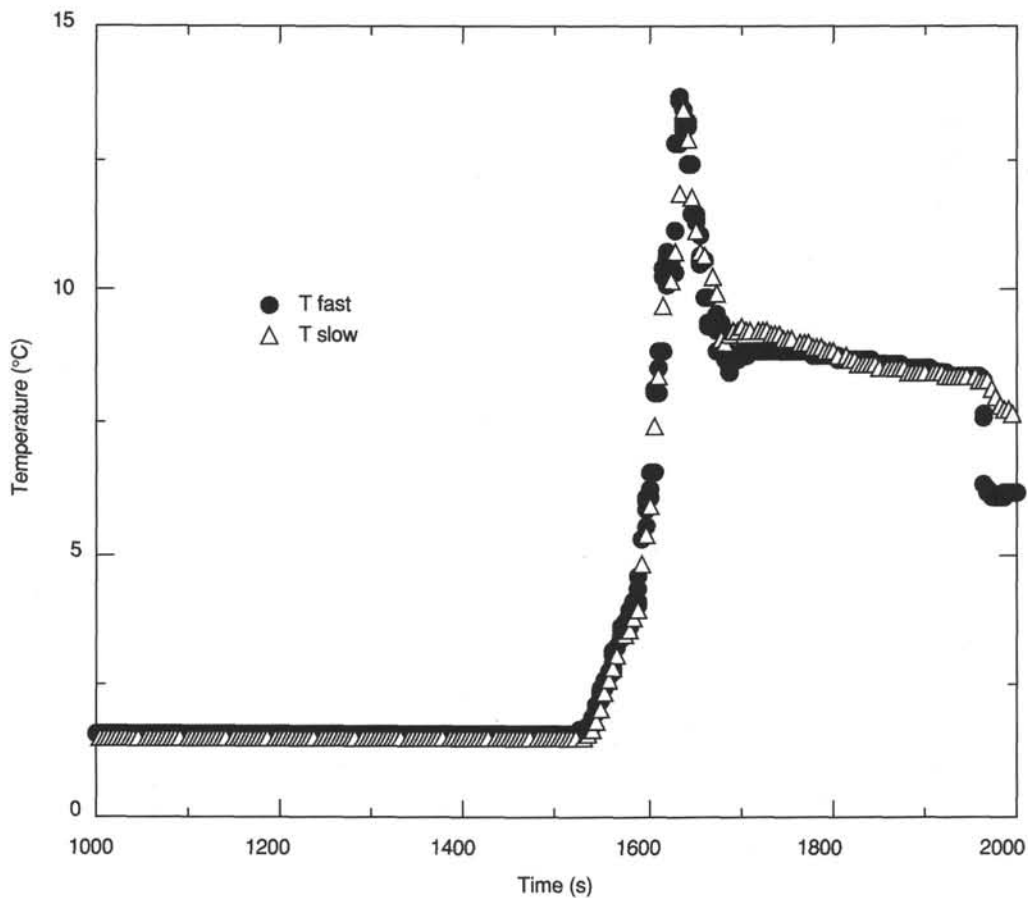


Figure 30. A comparison plot of the two thermistors vs. time. The differences after 1680 s are caused by a coating of mud on the slow-response thermistor.

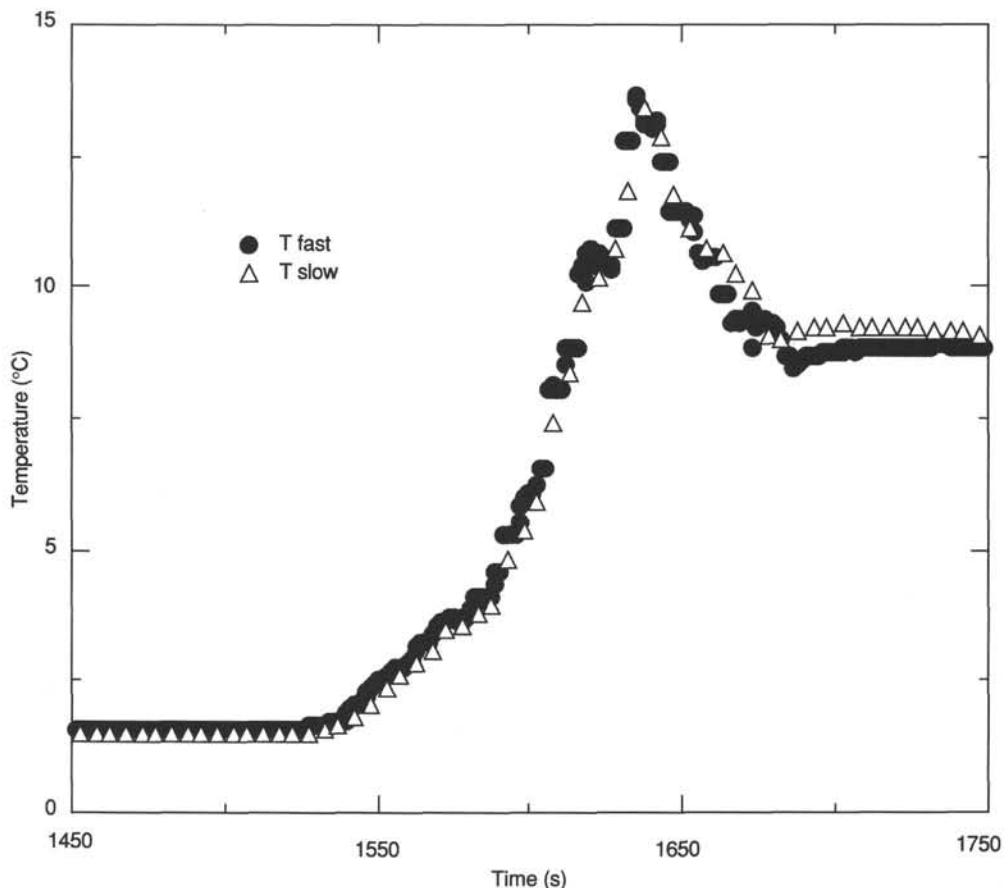


Figure 31. Plot similar to that in Figure 30, but with an expanded time scale. Note the difference in the slope between the interval from 1530 to 1590 s and the interval from 1590 to 1635 s.

temperature data is to plot temperature vs. the vertically integrated thermal resistance. We have plotted the thermal resistivity (the inverse of thermal conductivity) values for Site 780 in Figure 39. The integrated thermal resistivity is plotted vs. depth in Figure 40. The decreased slope of the line below 50 mbsf results from the higher thermal conduc-

tivity of the deeper sediments (Fig. 38). A good way of looking at this figure is to understand that for a constant heat flow, the temperature-vs.-depth curve will be proportional to this curve.

Temperature data from the two Barnes-Uyeda runs and the TLT value for the seafloor water temperature have been plotted vs. integrated thermal resistivity in Figure 41. The slope of the linear least-squares regression is the heat flow at this site, 52 mW/m².

Interestingly, the temperatures at depth in Hole 780D are much lower than the corresponding temperatures in Hole 780C. We interpret this phenomenon as revealing that temperatures in Hole 780C do not necessarily represent equilibrium conductive heat flow. Sediment/fluid geochemical results from Site 780 indicate that pore fluids must be moving upward within the sediments (see "Sediment/Fluid Geochemistry" section, this chapter). We speculate that the drillhole provided a conduit that allowed higher temperature fluids to escape. The high overpulls at 234 mbsf, about 130 mbsf, may represent a zone of higher fluid flow rates and higher fluid overpressures, which were forcing the formation into the hole at that depth.

SUMMARY AND CONCLUSIONS

Site 780 is situated on the west-southwest side of the summit of Conical Seamount at a depth of 3100 m, in an area shown by *Alvin* submersible dives to be sediment covered and marked by active venting of fluids and precipitation of material from solution. Four holes were drilled at this site: Hole 780A, which was APC-cored to 3.5 mbsf; Hole 780B, which

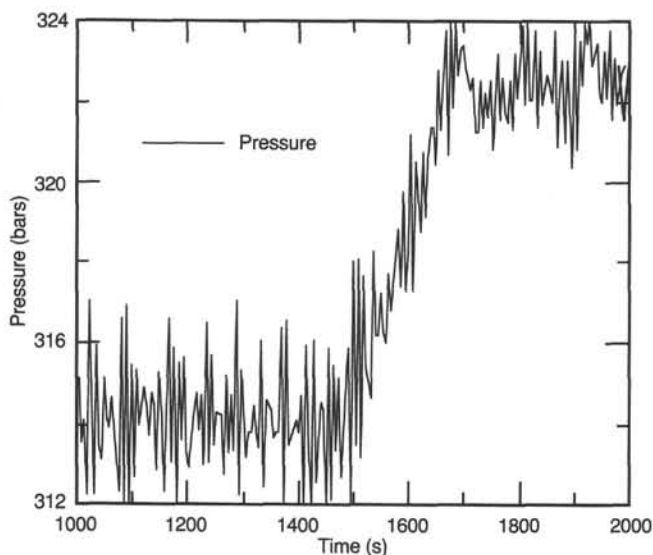


Figure 32. Plot of pressure (bars) vs. time as measured by the TLT.

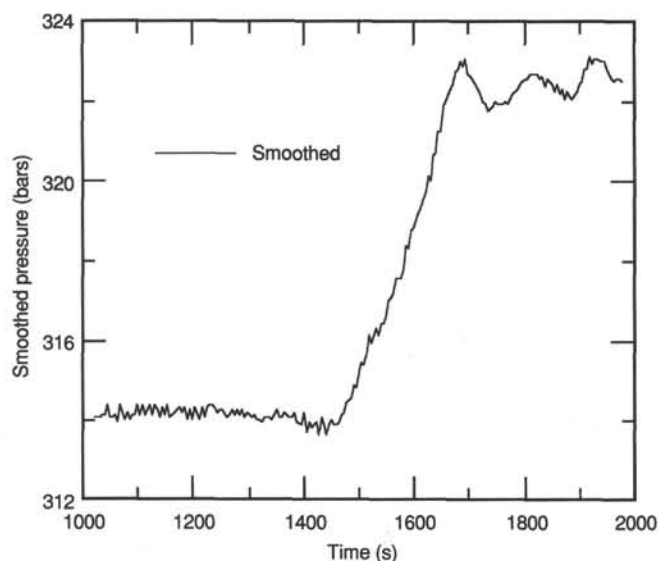


Figure 33. Plot similar to that in Figure 32, but with the pressure signal smoothed. Note that there is no dramatic change in slope at 1590 s, as there was in the temperature data.

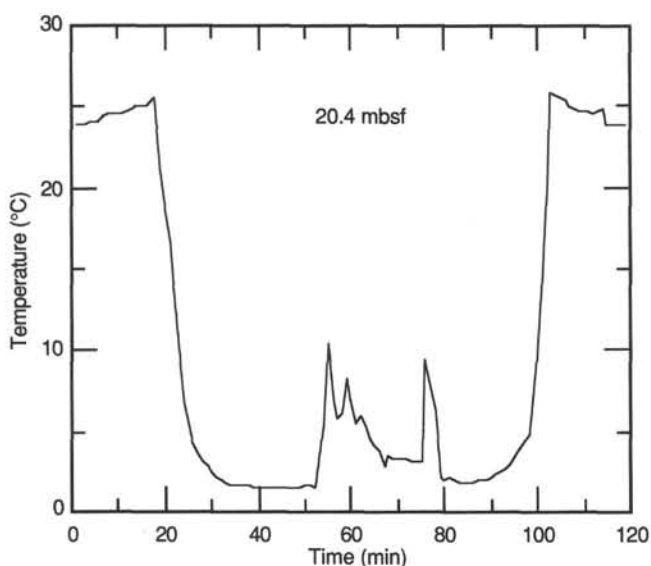


Figure 34. Temperature vs. time for the first Barnes-Uyeda temperature tool Run 06X at 20.4 mbsf. The probe was held stationary near the seafloor between 40 and 50 min into the run. It was firmly seated in the sediment between 59 and 76 min.

was RCB-cored to 18.2 mbsf; Hole 780C, which was RCB-cored to 163.5 mbsf; and Hole 780D, which was XCB-cored to 32.4 mbsf (Fig. 42). Recovery rates were low because of the interbedding of hard serpentinized peridotite and very soft unconsolidated serpentine.

Two major lithostratigraphic units were recovered at Site 780, as follows:

1. Unit I (0–3.5 mbsf in Hole 780A; 0–18.2 mbsf in Hole 780B; 0–14.0 mbsf in Hole 780C; and 0–15.4 mbsf in Hole 780D) comprises middle Pleistocene(?) to Holocene(?) sand- and silt-sized serpentine, with rare intervals of foraminifer-rich serpentine clay and serpentine-rich silty-clay; and

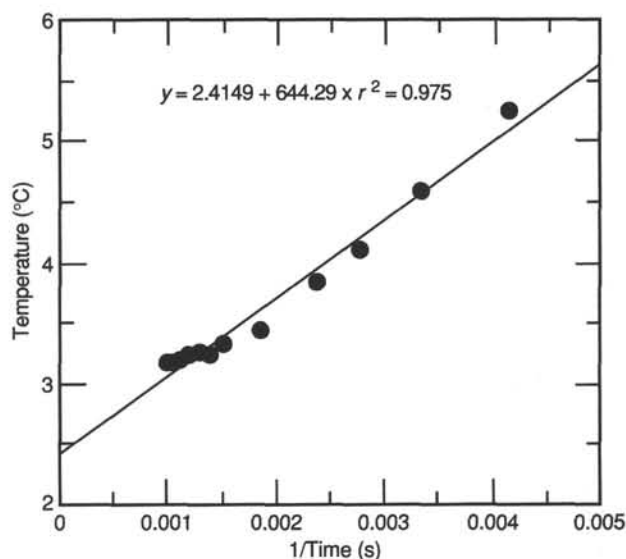


Figure 35. Reduced-temperature fit of the first Barnes-Uyeda temperature run. The intercept value at $1/\text{time} = 0$ is the equilibrium temperature of the sediment.

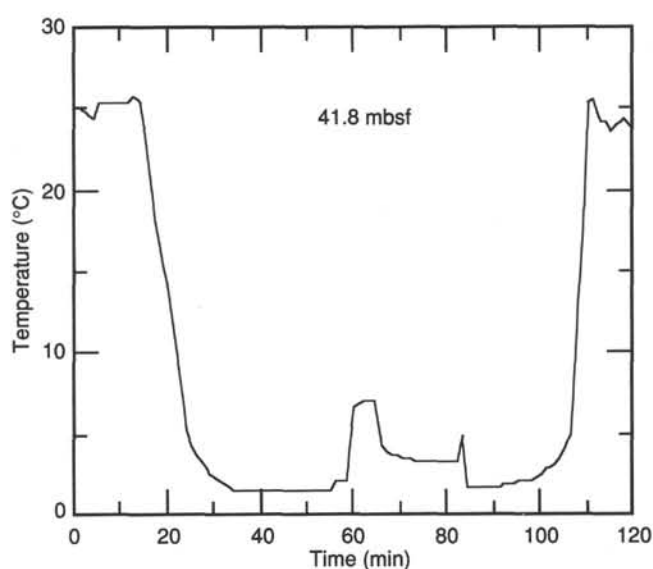


Figure 36. Plot of temperature vs. time for the second Barnes-Uyeda temperature tool Run 08X at 41.8 mbsf. The probe was firmly seated in the sediment between 63 and 81 min. There was less disturbance while the probe was in the sediment than occurred during the first run.

2. Unit II (14.0–163.5 mbsf in Hole 780C and 15.4–32.4 mbsf in Hole 780D) comprises intervals of serpentinized ultramafic rocks in a matrix of sandy silt- and clayey silt-sized serpentine.

The sediments in Unit I contain 65% to 75% serpentine, with minor amounts of opaque minerals, aragonite, and foraminifers and with trace amounts of zoisite, chlorite, nannofossils, spicules, silicoflagellates, diatoms, and radiolarians. Dating at Site 780 is based on the ages of calcareous nannofossils and planktonic foraminifers, which are middle to late Pleistocene in the upper portions of Holes 780A, 780B, 780C and 780D. The presence of delicate aragonite needles implies authigenic growth after the serpentine was emplaced. The

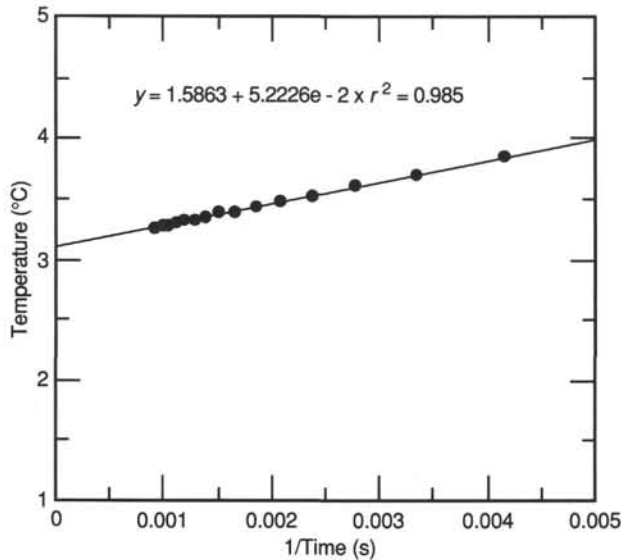


Figure 37. The corresponding reduced temperature fit for the second Barnes-Uyeda run. Notice the improved quality of the fit.

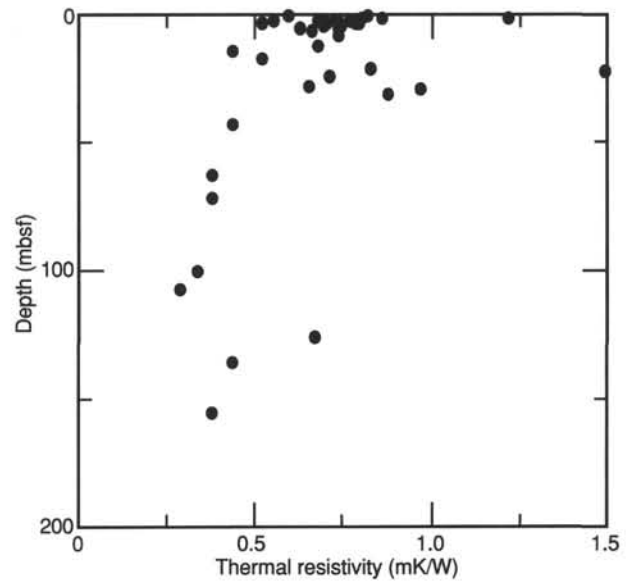


Figure 39. Plot similar to that in Figure 38, except that the value is thermal resistivity (mK/W), the inverse of thermal conductivity.

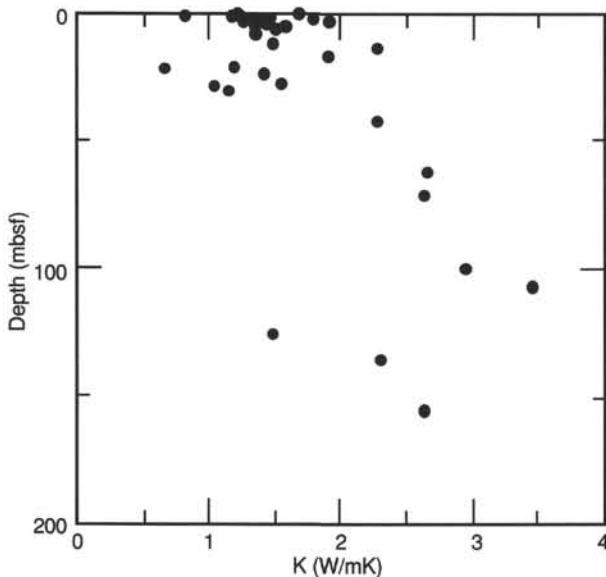


Figure 38. The combined thermal conductivity results (W/mK) for Holes 780A through 780D plotted vs. depth.

matrix in Unit II contains 70% to 99% serpentine, with minor to trace amounts of opaque minerals, clay minerals, zoisite, chlorite, micrite, and garnet.

Hard-rock lithologies constitute serpentinized, tectonized ultramafic rocks, and subordinate serpentinized dunites having similar primary mineralogies to the ultramafic rocks from Sites 778 and 779. Serpentine veins are common and show a polystage filling history. The muddy matrix recovered from Site 780 typically lacks the foliation and shear fabric of the matrix from the flank sites; thus, this matrix may be interpreted as the primary fabric of the upwelling serpentinite, upon which foliation and shear fabric have been imposed by compaction, extension, and pure shear during the downhill creep of serpentinite debris flows.

Logging in Hole 780C showed that temperatures increased steadily from seawater values (1.5°C) near the surface to 13.5°C at 60 mbsf; the WSTP in Hole 780D gave the lower value of

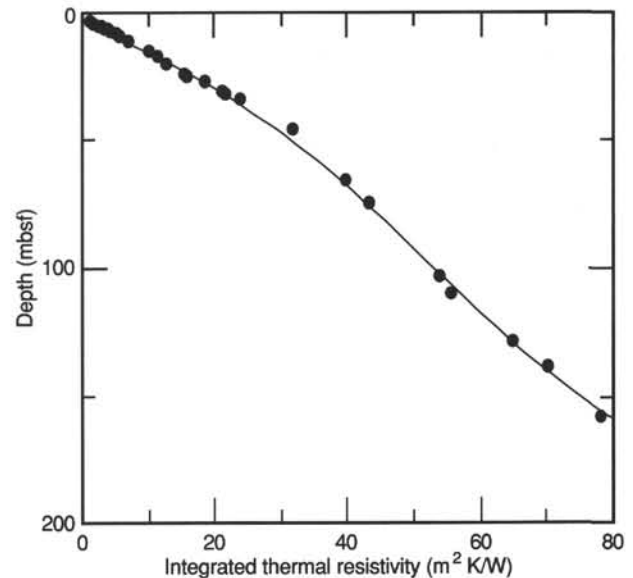


Figure 40. Integrated thermal resistivity, the depth integral of thermal resistivity (m²K/W), plotted vs. depth.

3.15°C at 41 mbsf, and an estimated heat flow of 52 mW/m². Studies of physical properties give a density range of 1.75 to 2.0 g/cm³ and compressional-wave velocities of 1.5 to 2 km/s for the serpentine-rich matrix in Unit II. Rheological measurements indicate that this matrix is a weak, highly non-ideal, plastic material capable of supporting blocks up to 20 m wide, and it is compatible with models for diapiric injection of the serpentinite.

Analyses of interstitial pore-water samples at Site 780 revealed marked downhole chemical changes. Holes 780A and 780D show the greatest variation: salinity decreases by 25%, chlorinity by 20%, calcium by 90%; magnesium is totally depleted, sulfate nearly doubles, alkalinity increases from 2.5 to 34, pH increases from about 8 to 12.4, potassium increases significantly, and ammonia increases dramatically. These changes take place within a few meters of the seafloor,

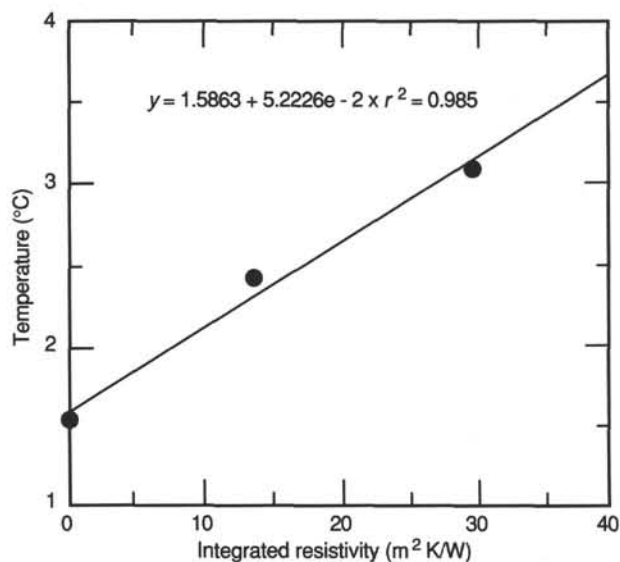


Figure 41. Plot of temperature vs. integrated thermal resistivity. The slope of the best-fitting linear regression is the heat flow value of 52 mW/m².

showing that the fluid entrained within the serpentinite may mix only with seawater at very shallow levels. The magnitude and direction of these changes also differs in significant ways when compared to the flank sites.

The principal results of Site 780 can be summarized as follows:

1. High pH, high alkalinity, very low magnesian fluids may exist within a few meters of the seafloor at the summit of Conical Seamount, indicating that mixing of entrained fluids and seawater need not take place at depth.

2. Rheological studies support a model for the origin of the seamount by diapiric intrusion of variably serpentinitized clasts supported by a low-density, plastic matrix.

3. Absence of deformation in the serpentinite matrix at the summit contrasts with the strongly sheared matrix at the flanks and suggests that much of the deformation of the serpentinite matrix at the flank sites was the result of surface or near-surface flow following diapiric intrusion.

REFERENCES

- Backman, J., Duncan, R. A., et al., 1988. Explanatory Notes. *Proc. ODP, Init. Repts.*, 115: College Station, TX (Ocean Drilling Program), 17-42.
- Berger, W. H., 1970. Planktonic foraminifera: selective solution and the lysocline. *Mar. Geol.*, 8:1-11.
- Berner, R. A., and Honjo, S., 1981. Pelagic sedimentation of aragonite: its geochemical significance. *Science*, 211:940-942.
- Fryer, P., et al., 1987. Results of *Alvin* studies of Mariana forearc serpentinite diapirism. *EOS, Trans. Am. Geophys. Union*, 68:1534.
- Gieskes, J. M., Johnston, K., and Boehm, M., 1985. Interstitial water studies, Leg 66. In von Huene, R., Aubouin, J., et al., *Init. Repts. DSDP*, 67: Washington (U.S. Govt. Printing Office), 961-967.
- Haggerty, J. A., 1987a. Petrology and geochemistry of Neogene sedimentary rocks from Mariana forearc seamounts: implications for emplacement of the seamounts. In Keating, B., Fryer, P., Batiza, R., and Bohlert, G. (Eds.), *Seamounts, Islands and Atolls*: Washington (Am. Geophys. Union) Monogr. Ser., 43:175-185.
- _____, 1987b. Geochemistry of carbonate and silicate chimney structures from Conical Seamount collected during *Alvin* dive studies. *EOS, Trans. Am. Geophys. Union*, 68:1534.

Age	Hole 780C			Lithology
	Core	Recovery	Lith. units	
Holocene to middle Pleistocene	1R		I	Sand- and silt-sized serpentinite
	2R			
	3R			
(?)	4R		Serpentinized harzburgite and dunite in a matrix of sand- and silt-sized serpentinite sediment	
	5R			
	6R			
	7R			
	8R			
	9R			
	10R			
(?)	11R			II
	12R			
	13R			
	14R			
	15R			
	16R			
	17R			
	18R			

Figure 42. Summary of lithology and core recovery, Hole 780C.

- _____, 1987c. Cold-water, deep-sea chimneys from the Mariana forearc serpentinite seamounts (Abst.). *EOS, Trans. Am. Geophys. Union*, 68:1534.
- _____, 1989. Fluid inclusion studies of chimneys associated with serpentinite seamounts in the Mariana forearc (Abst.). *PACROFI II*, 2:29.
- Harrison, W. E., Hesse, R., and Gieskes, J. M., 1982. Relationship between sedimentary facies and interstitial water chemistry of slope, trench, and Cocos plate sites from the Middle America Trench transect, active margin off Guatemala, Deep Sea Drilling Project Leg 67. In Aubouin, J., von Huene, R., et al., *Init. Repts. DSDP*, 67: Washington (U.S. Govt. Printing Office), 603-613.
- Hesse, R., Lebel, J., and Gieskes, J. M., 1985. Interstitial water chemistry of gas-hydrate-bearing sections on the Middle America Trench slope, Deep Sea Drilling Project Leg 84. In von Huene, R., Aubouin, J., et al., *Init. Repts. DSDP*, 84: Washington (U.S. Govt. Printing Office), 727-737.
- Hussong, D. M., and Uyeda, S., 1981. Tectonic processes and the history of the Mariana arc: A synthesis of the results of Deep Sea Drilling Project Leg 60. In Hussong, D. M., Uyeda, S., et al., *Init. Repts. DSDP*, 60: Washington (U.S. Govt. Printing Office), 909-929.
- Janecky, D. R., and Seyfried, W. E., Jr., 1986. Hydrothermal serpentinitization of peridotite within the oceanic crust: experimen-

- tal investigations of mineralogy and major element chemistry. *Geochim. Cosmochim. Acta*, 50:1357-1378.
- Kohls, D. W., and Rodda, J. L., 1967. Iowaite, a new hydrous magnesium hydroxide-ferric oxychloride from the Precambrian of Iowa. *Am. Mineral.*, 52:1261-1271.
- Kulm, L. D., Suess, E., Moore, J. C., Carson, B., Lewis, B. T., Ritger, S. D., Kadko, D. C., Thornburg, T. M., Embley, R. W., Rugh, W. D., Massoth, G. J., Langseth, M. G., Cochrane, G. R., and Scamman, R. L., 1986. Oregon subduction zone: venting, fauna, and carbonates. *Science*, 231:561-566.
- Li, Y.-H., Takahashi, T., and Broecker, W. S., 1969. Degree of saturation of calcium carbonate in the oceans. *J. Geophys. Res.*, 75:5507-5525.
- Miura, Y., Rucklidge, J. C., and Nord, G. L., Jr., 1981. The occurrence of chlorine in serpentine minerals. *Contrib. Mineral. Petrol.*, 76:17-23.
- Moore, G. W., and Gieskes, J. M., 1980. Interaction between sediment and interstitial water near the Japan Trench, Leg 57, Deep Sea Drilling Project. In Scientific Party, von Huene, R., and Nasu, N., *Init. Repts. DSDP*, 56, 57 (Pt. 2): Washington (U.S. Govt. Printing Office), 1269-1275.
- Okada, H., and Bukry, D., 1980. Supplementary modification and introduction of code numbers to the low-latitude coccolith biostratigraphic zonation (Bukry, 1973; 1975). *Mar. Micropaleontol.*, 5:321-325.
- Phipps, S. P., 1984. Mesozoic ophiolitic olistostromes and Cenozoic imbricate thrust faulting in the northern California coast ranges; geology of the Mysterious Valley, Napa County [Ph.D. dissert.]. Princeton Univ., Princeton, NJ.
- Poty, B., Holland, H. D., and Borcsik, M., 1972. Solution-mineral equilibria in the system MgO-SiO₂-H₂O-MgCl₂ at 500°C and 1 kbar. *Geochim. Cosmochim. Acta*, 36:1101-1113.
- Rucklidge, J. C., 1972. Chlorine in partially serpentinized dunite. *Econ. Geol.*, 67:38-40.
- Rucklidge, J. C., and Patterson, G. C., 1977. The role of chlorine in serpentinization. *Contrib. Mineral. Petrol.*, 65:39-44.
- Schorno, K. S., 1981. Geochemistry of carbon, International Phase of Ocean Drilling Project Leg 60. In Hussong, D. M., Uyeda, S., et al., *Init. Repts. DSDP*, 60: Washington (U.S. Govt. Printing Office), 501-504.
- Shipboard Scientific Party, 1988a. Synthesis of shipboard results: Leg 110 transect of the Northern Barbados Ridge. In Masle, A., Moore, J. C., et al., *Proc. ODP, Init. Repts.*, 110: College Station, TX (Ocean Drilling Program), 577-591.
- Shipboard Scientific Party, 1988b. Introduction, objectives, and principal results, Leg 112, Peru continental margin. In Suess, E., von Huene, R., et al., *Proc. ODP, Init. Repts.*, 112: College Station, TX (Ocean Drilling Program), 5-23.

Ms 125A-108

NOTE: All core description forms ("barrel sheets") and core photographs have been printed on coated paper and bound as Section 4, near the back of the book, beginning on page 383.